

APPLIED INFORMATION SYSTEMS RESEARCH (AISR) PROGRAM

**Second Annual Report for AISR Grant NNG06EC81I**  
***Parallel-Processing Astrophysical Image-Analysis Tools***  
**April 1, 2007 to March 30, 2008 (Year 2 of 3)**

PI: Kenneth J. Mighell (National Optical Astronomy Observatory)

During the past year, the Principal Investigator (PI) has worked closely with Bill Hoffmann (Steward Observatory) and Bill Glaccum (Caltech/Spitzer Science Center), both members of the *Spitzer Space Telescope's* Infrared Array Camera (IRAC) Instrument Team, to demonstrate that his AISR-funded MATPHOT algorithm [1] for precision stellar photometry and astrometry can yield an improvement in the precision of stellar photometry obtained from IRAC Ch1 observations of bright stars of more than 100% over the best results obtained with aperture photometry using the calibration procedures recommended in the IRAC Data Handbook[2].

This research effort has now been recognized by the Spitzer Science Center. Mighell (PI), Hoffman, & Glaccum received a small Spitzer Cycle-4 grant *Improving the Photometric Precision of IRAC Channels 1 & 2* (Archival Research Proposal #40106) to analyze archival observations of bright stars obtained with IRAC Ch1 and Ch2 with the goal of developing new calibration and analysis procedures that have the potential of significantly improving the precision of point-source photometry. This timely research effort is intended to enhance the science return not only of existing IRAC Ch1 and Ch2 observations in the Spitzer data archive but also those that will be made during the possible Spitzer Warm Mission which would start around April 2009 after all of the cryogen is depleted.

The PI presented a 30 minute talk *Improving the Precision of Near-Infrared Stellar Photometry by Modeling the Image Formation Process within a Lossy Detector* [3] on Wednesday June 20, 2007 at the 2007 NASA Science Technology Conference (NSTC2007) which was held at the University of Maryland University College on June 19–21, 2007. A detector can be considered to be effectively lossy if a pixel, the smallest optically sensitive unit of the detector, internally exhibits a non-uniform response function that has a quantum efficiency variation with an rms dispersion exceeding an arbitrary level of 1%. Near-infrared astronomical cameras based on lossy detectors can have large systematic errors in the measurement of total stellar flux if stellar images are undersampled. While this problem can be mitigated by oversampling the stellar image, many near-infrared cameras are deliberately undersampled in order to achieve a large field of view. The PI demonstrated that although the recorded flux from undersampled stellar observations can be corrupted by using detectors with significant effective intrapixel quantum efficiency variations, it is still possible to achieve excellent stellar photometry with an existing space-based near-infrared camera (IRAC) – if the image formation process *inside the detector* is accurately modeled using a new experimental version of the MATPHOT code called MPDZ.

The PI presented a 20 minute talk *Enhancing the Science Return of the Spitzer Warm Mission*[4] on Thursday September 13, 2007 at the 2007 Advanced Maui Optical and Space Surveillance Technologies Conference (AMOS2007) which was held in Wailea, Maui, Hawaii on September 12–15, 2007. The PI described how the science return of the Spitzer Warm Mission could be enhanced using the MATPHOT code on IRAC Channel 1 observations. The PI presented a new *two-dimensional* aperture-photometry flux correction based on computed MPDZ Point Response Function (PRF) volumes of 100,000 artificial stellar observations (see Fig. 1). The PI demonstrated that the new two-dimensional flux correction yields an improvement of 100% over the standard correction given in the IRAC Data Handbook when given accurate centroid estimates.

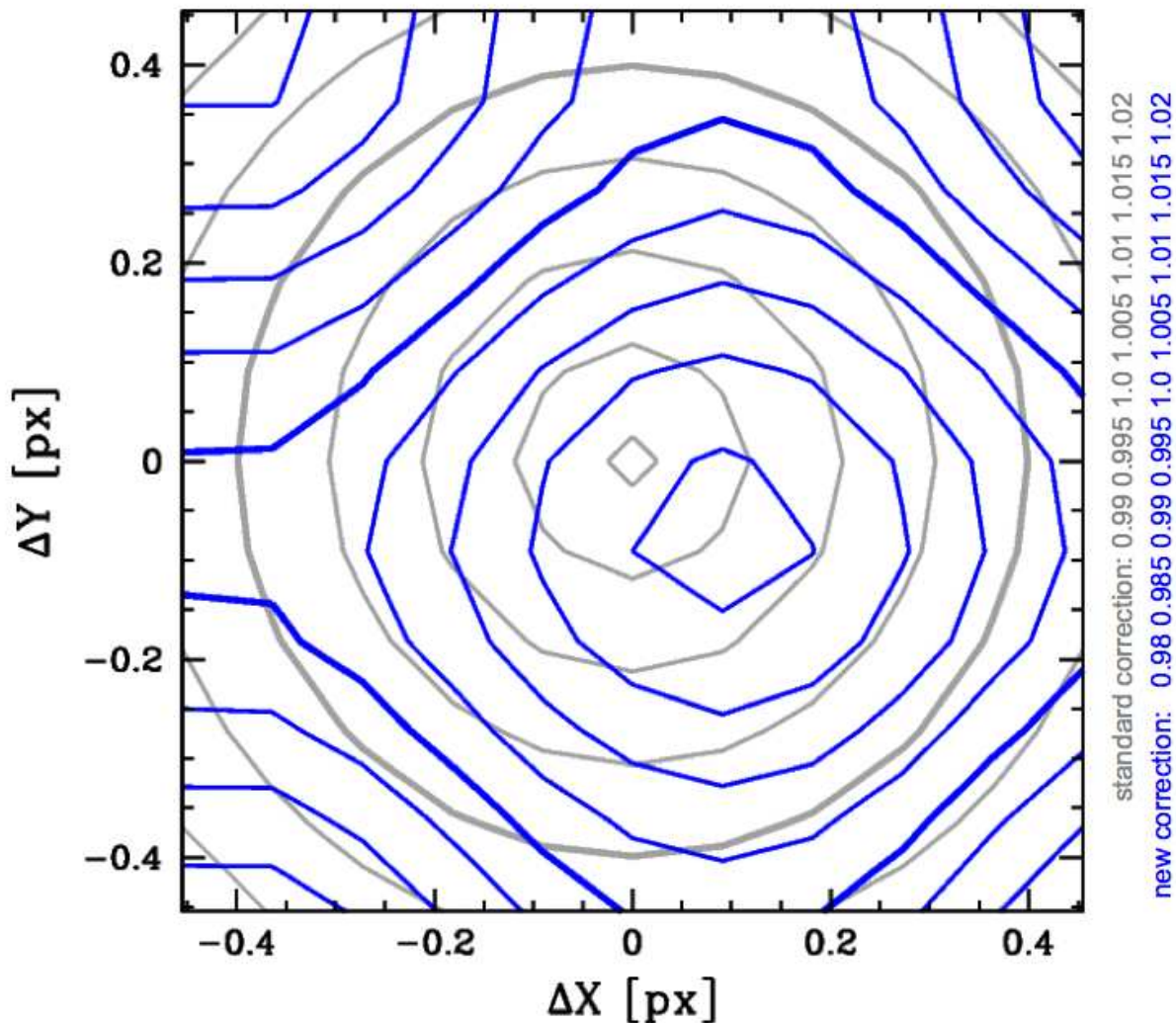


Figure 1: Comparison of the PI's new aperture flux correction (blue contours) with the aperture flux correction from the IRAC Data Handbook (gray contours). The contours of the standard correction range from 99 to 102% in steps of 0.5%; the contours of the new correction range from 98 to 102% in steps of 0.5%.

## SECOND ANNUAL REPORT FOR AISR GRANT NNG06EC81I (PI: MIGHELL)

The PI, Glaccum, and Hoffmann have been invited to give a poster presentation on June 23, 2008 at the SPIE-Marseille (June 23–28, 2008) [5] conference on Space Telescopes and Instrumentation I: Optical, Infrared, and Millimeter. We will present our analysis of archival observations of calibration stars and compare the precision of stellar aperture photometry, with one-dimensional and two-dimensional pixel-phase flux corrections, and MATPHOT-based PRF-fitting photometry which accounts for the observed loss of stellar flux due to the nonuniform intrapixel quantum efficiency (see Fig. 2). We will show how the precision of aperture photometry of bright stars calibrated with a 2-dimensional correction function, based on simulations made with the PI's new MPDZ code, can yield photometry that is almost as precise as that produced by PSF-fitting procedures. We will describe how the precision photometry made possible with the MATPHOT code could be used to do more precise studies of exoplanets, white dwarfs, variable stars, and searches of T dwarf companions during the possible Spitzer Warm Mission.

**MySPIE** User: mighell  
Sign out Web Account Help SPIE.org

MySPIE Home > Review and Submit

**SUBMIT AN ABSTRACT REVIEW AND SUBMIT**

**Presentation: Improving the Photometric Precision of IRAC Channel 1**  
Conference: Space Telescopes and Instrumentation I: Optical, Infrared, and Millimeter  
Symposium: AS08 Astronomical Telescopes and Instrumentation: Synergies Between Ground and Space

① Overview ② Authors ③ Abstract ④ **Review and Submit**

**Primary Author:**  
Mighell, Kenneth National Optical Astronomy Observatory mighell@noao.edu

**Co-Authors:**  
Glaccum, William Caltech/Spitzer Science Center glaccum@ipac.caltech.edu  
Hoffmann, William Steward Observatory/University of Arizona whoffmann@as.arizona.edu

**Contact Person:**  
Mighell, Kenneth National Optical Astronomy Observatory mighell@noao.edu

**Abstract Text for Online or Printed Programs:**

**Abstract Text for Technical Review Purposes:**  
Planning is underway for a possible post-cryogenic mission with the Spitzer Space Telescope. Only Channels 1 and 2 (3.6 and 4.5 microns) of the Infrared Array Camera (IRAC) will be operational; they will have unmatched sensitivity from 3 to 5 microns until the James Webb Space Telescope is launched. At SPIE Orlando, Mighell described his NASA-funded MATPHOT algorithm for precision stellar photometry and astrometry and presented MATPHOT-based simulations that suggested Channel 1 stellar photometry may be significantly improved by modeling the nonuniform RQE within each pixel, which, when not taken into account in aperture photometry, causes the derived flux to vary according to where the centroid falls within a single pixel (the pixel-phase effect). We analyze archival observations of calibration stars and compare the precision of stellar aperture photometry, with 1-dimensional and 2-dimensional pixel-phase flux corrections, and MATPHOT-based PSF-fitting photometry which accounts for the observed loss of stellar flux due to the nonuniform intrapixel quantum efficiency. We show how the precision of aperture photometry of bright stars corrected with a 2-dimensional correction function can yield photometry that is almost as precise as that produced by PSF-fitting procedures. This timely research effort is intended to enhance the science return not only of observations already in Spitzer data archive but also those that will be made during the Spitzer Warm Mission.

<< PREVIOUS CANCEL FINISH

Telephone: +1 360 676 3290 | Fax: +1 360 647 1445 | Email: [myspiehelp@spie.org](mailto:myspiehelp@spie.org)  
© 1994–2007 SPIE—The International Society for Optical Engineering  
Mon-Fri 8am to 5pm, Pacific Time.

Figure 2: Abstract of our poster presentation on June 23, 2008 at the SPIE-Marseille conference on Space Telescopes and Instrumentation I: Optical, Infrared, and Millimeter.

While many astronomical image analysis tasks are based on algorithms that can be described as being *embarrassingly parallel*, where the analysis of one subimage generally does not affect the analysis of another subimage, few parallel-processing astrophysical image-analysis programs exist that can easily take full advantage of today's fast multi-core servers costing a few thousands of dollars. One of the key reasons for this shortage of state-of-the-art parallel-processing astrophysical image-analysis codes is that the writing of parallel codes has been perceived to be difficult.

As part of AISR-funded research, the PI is developing a new software framework to greatly simplify the process of creating useful parallel-processing astrophysical image analysis codes based on embarrassingly-parallel algorithms.

The first application of this new software framework is a new fast parallel-processing image-analysis program called CRBLASTER which does cosmic ray rejection using van Dokkum's L.A.Cosmic algorithm [6]. CRBLASTER is written in C using the industry standard Message Passing Interface library. Figure 3 shows the cosmic-ray damaged long-exposure (2400 sec) *Hubble Space Telescope* WFPC2 observation of the galaxy cluster MS 1137+67; the right image shows how CRBLASTER has effectively eliminate almost all cosmic rays present in the original observation.

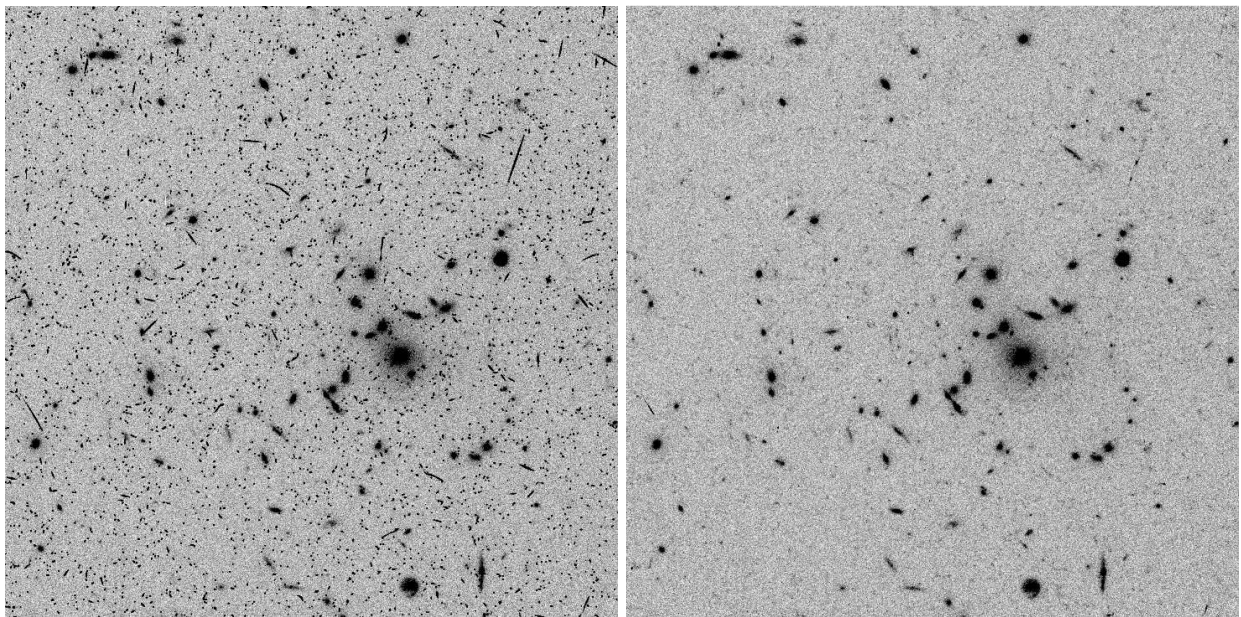


Figure 3: The left image shows a portion of a 2400-sec *Hubble Space Telescope* WFPC2 observation of the galaxy cluster MS 1137+67. The right image is the CRBLASTER-processed version of the original observation.

Processing a single 800×800 HST WFPC2 image takes 21 seconds with van Dokkum's original `lacos.im.cl` IRAF script on an Apple Xserve with two dual-core 3.0-GHz Intel Xeon CPUs. CRBLASTER takes just 1.87 seconds using all 4 cores; the efficiency of the program running with the 4 processors is an excellent 82% (see Fig. 4).

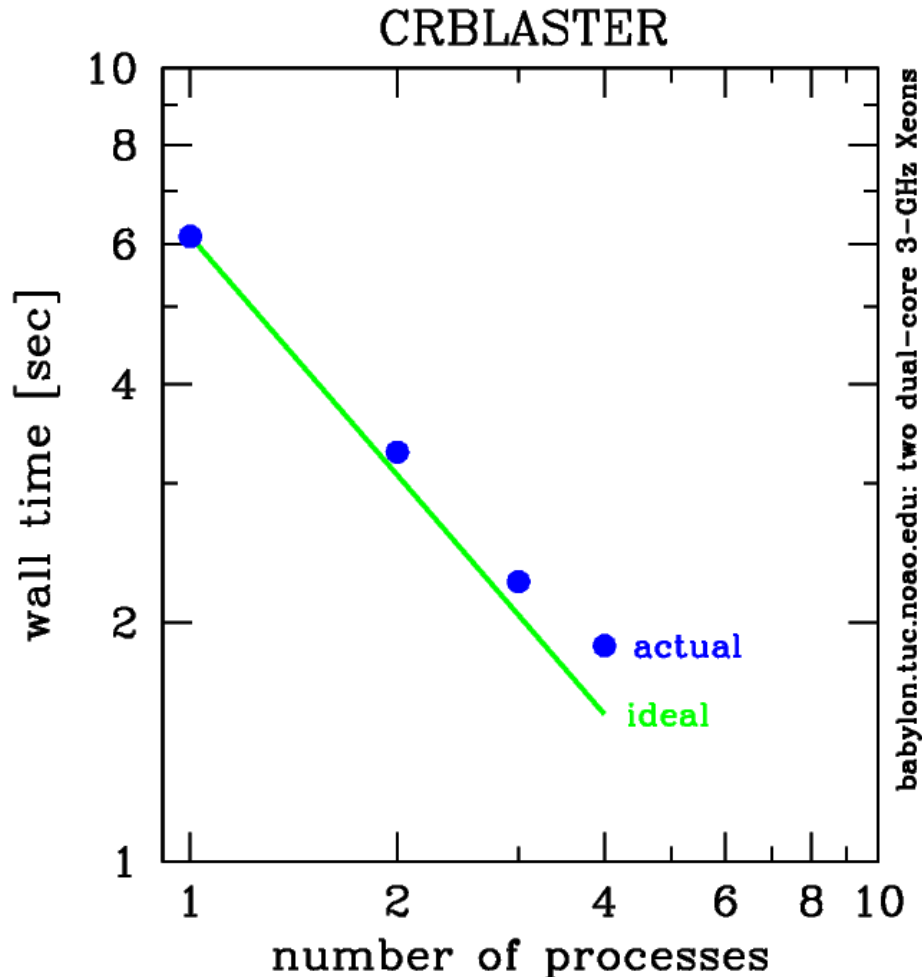


Figure 4: Total execution time (wall time) as a function of the number of processes for the CRBLASTER application compared with the ideal model of a purely parallel algorithm. CRBLASTER takes just 1.87 seconds using all 4 cores of an Apple Xserve with two dual-core 3.0-Ghz Intel Xeon CPUs – an excellent efficiency of 82%.

CRBLASTER can be used as a software framework for the easy development of parallel-processing image-analysis programs using embarrassing parallel algorithms; all that needs to be done is to replace the core image processing task (in this case the C-version of the L.A.Cosmic algorithm) with an alternative image analysis task based on a single-processor algorithm.

The PI has been invited to give the oral presentation *CRBLASTER<sup>1</sup>: A Fast Parallel-Processing Program for Cosmic Ray Rejection* on June 28, 2008 at the SPIE-Marseille conference on *Advanced Software and Control for Astronomy* (see Fig. 5). The PI will describe the design and implementation of CRBLASTER and then discuss how it could possibly be used to quickly do complex calibration tasks as part of the pipeline processing of images from large focal plane arrays.

---

<sup>1</sup>The name of the application has recently been changed from CRFIND to CRBLASTER as the original name was discovered to not be unique.



## SECOND ANNUAL REPORT FOR AISR GRANT NNG06EC81I (PI: MIGHELL)

The screenshot shows the MySPIE website interface. At the top, there is a navigation bar with the MySPIE logo, user information (User: mighell), and links for Sign out, Web Account, and Help. Below this is a breadcrumb trail: MySPIE Home > Review and Submit. The main content area is titled 'SUBMIT AN ABSTRACT REVIEW AND SUBMIT'. It displays the presentation title 'CRFIND: A Fast Parallel-Processing Program for Cosmic Ray Rejection', the conference 'Advanced Software and Control for Astronomy', and the symposium 'AS08 Astronomical Telescopes and Instrumentation: Synergies Between Ground and Space'. A progress bar shows four steps: 1 Overview, 2 Authors, 3 Abstract, and 4 Review and Submit (which is highlighted). Below the progress bar, it lists the Primary Author as Mighell, Kenneth National Optical Astronomy Observatory, with email mighell@noao.edu. It also lists Co-Authors and Contact Person. The Abstract Text for Online or Printed Programs is provided, followed by the Abstract Text for Technical Review Purposes, which describes the CRFIND program. At the bottom of the form are three buttons: PREVIOUS, CANCEL, and FINISH. Below the form, contact information for SPIE is provided: Telephone: +1 360 676 3290, Fax: +1 360 647 1445, Email: mysplehelp@spie.org, and copyright information for 1994-2007 SPIE.

MySPIE User: mighell Sign out Web Account Help SPIE.org

MySPIE Home > Review and Submit

**SUBMIT AN ABSTRACT REVIEW AND SUBMIT**

**Presentation: CRFIND: A Fast Parallel-Processing Program for Cosmic Ray Rejection**  
Conference: Advanced Software and Control for Astronomy  
Symposium: AS08 Astronomical Telescopes and Instrumentation: Synergies Between Ground and Space

① Overview ② Authors ③ Abstract ④ **Review and Submit**

**Primary Author:**  
Mighell, Kenneth National Optical Astronomy Observatory mighell@noao.edu

**Co-Authors:**

**Contact Person:**  
Mighell, Kenneth National Optical Astronomy Observatory mighell@noao.edu

**Abstract Text for Online or Printed Programs:**

**Abstract Text for Technical Review Purposes:**  
Many astronomical image analysis tasks are based on algorithms that can be described as being "embarrassingly parallel", where the analysis of one subimage generally does not affect the analysis of another subimage. Yet few parallel-processing astrophysical image-analysis programs exist that can easily take full advantage of today's fast multi-core servers costing a few thousands of dollars. The main reason for the shortage of state-of-the-art parallel-processing astrophysical image-analysis codes is that the writing of parallel codes has been perceived to be difficult. I describe a new fast parallel-processing image-analysis program called CRFIND which does cosmic ray rejection using van Dokkum's L.A.Cosmic algorithm. CRFIND is written in C using the industry standard Message Passing Interface library. Processing a single 800x800 HST WFPC2 image takes 1.87 seconds using 4 processes on an Apple Xserve with two dual-core 3.0-GHz Intel Xeons; the efficiency of the program running with the 4 processors is 82%. The code can be used as a software framework for easy development of parallel-processing image-analysis programs using "embarrassing parallel" algorithms; all that needs to be done is to replace the core image processing task (in this case the C-version of the L.A.Cosmic algorithm) with an alternative image analysis task based on a single-processor algorithm. I describe the design and implementation of the program and then discuss how it could possibly be used to quickly do complex calibration tasks as part of the pipeline processing of images from large focal plane arrays.

PREVIOUS CANCEL FINISH

Telephone: +1 360 676 3290 | Fax: +1 360 647 1445 | Email: [mysplehelp@spie.org](mailto:mysplehelp@spie.org)  
© 1994-2007 SPIE—The International Society for Optical Engineering  
Mon-Fri 8am to 5pm, Pacific Time.

Figure 5: Abstract of the PI's oral presentation on June 28, 2008 at the SPIE-Marseille conference on Advanced Software and Control for Astronomy.

The PI met Dr. John Samson who is the Principal Investigator of NASA's New Millennium Program (NMP) Space Technology 8 (ST8) Dependable Multiprocessor (DM) project (see Fig. 6) at the 2007 NASA Science Technology Conference last June. The goal of the DM project is to conduct a comprehensive research project to investigate and develop for NASA the first supercomputer in space [7].

Samson's team at Honeywell Aerospace (Clearwater, Florida) is partnering with High-performance Computing and Simulation (HCS) Research Laboratory (see Fig. 7) at the University of Florida (Gainesville, Florida) whose director and founder is Prof. Alan D. George.

Dependable Multiprocessor has been an ongoing NMP project since 2004. DM was one of the four technologies selected for the NMP ST8 flight experiment. To date, NASA has provided \$10M funding to the DM project. The DM project has been proceeding toward a flight validation experiment in 2009. DM cluster management and enhanced software-based SEU<sup>2</sup>-tolerance were shown at the TRL5<sup>3</sup> technology validation demonstration in May 2006. Radiation testing of key COTS (Commercial Off The Shelf) components selected for the flight experiment showed that these components exhibited no catastrophic latch-up and a sufficient number of SEUs to support the flight validation experiment. The DM project held a successful CDR (Critical Design Review) in

<sup>2</sup>SEU: Single Event Upset

<sup>3</sup>TRL5: Component and/or breadboard validation in relevant environment [8]

## **SECOND ANNUAL REPORT FOR AISR GRANT NNG06EC81I (PI: MIGHELL)**

---

June of 2007. In August 2007, NASA funding cuts eliminated the flight experiments from the ST8 project. As a result, the ST8 project will end with the ground-based TRL6<sup>4</sup> technology validation demonstrations currently scheduled to be completed no later than October 2008. The DM project is looking for an alternative ride to establish its space pedigree for use on future NASA missions.

At the CDR last June, the NASA Technology Review Board (TRB) identified the need for the DM project to work with researchers with parallel-processing scientific applications that would be suitable for use in NASA's first supercomputer in space. The TRB was concerned that the fault-tolerant middleware techniques implemented in the DM software framework might be too complicated for say, an astrophysicist, to use as opposed to a computer scientist.

At NSTC2007, Samson and the PI identified two of the PI's AISR-funded parallel-processing image-analysis astrophysical applications, QLWFPC2[9] and CRBLASTER, which would make good candidates for porting to the DM-sigma (see Fig. 8) software-testbed cluster with a (hopefully) minimum effort on the part of the PI. **The PI has just recently ported those two applications to the DM-sigma software-testbed cluster in under six hours apiece** (see Fig. 9).

The achievement of this DM project milestone goes a long way towards addressing the concerns of the NASA TRB about the true portability of existing parallel-processing scientific-analysis applications to the DM platform using the DM middleware approach of achieving a dependable space-based cluster based on COTS hardware *and* software components.

The PI looks forward to collaborating further with Samson and George on this very interesting project which has great potential to enable NASA's new astrophysical missions in the next decade to possibly have significantly greater computing processing power than can now be envisioned even for NASA's currently planned large missions like the *James Webb Space Telescope* which has a proposed launch date in June 2013. Software fault injection experiments on DM-porting scientific applications running on the DM-sigma software-testbed cluster will begin in mid-March 2008. Radiation tests of the TRL6 hardware testbed are currently scheduled for mid-June 2008.

The PI presented a 15 minute talk *The Lost Flux Method: A New Algorithm for Improving the Precision of Space-Based Near-Infrared Stellar Photometry with Lossy Detectors* on Monday October 16, 2006 at the Astronomical Data Analysis Software and Systems XVI which was held in Tucson, Arizona on October 15-18, 2006. The ADASS 2006 conference proceedings, with a 4 page article by the PI with the same title as the talk, was published in October 2007 [10].

---

<sup>4</sup> TRL6: System/subsystem model or prototype demonstration in a relevant environment (ground or space) [8]

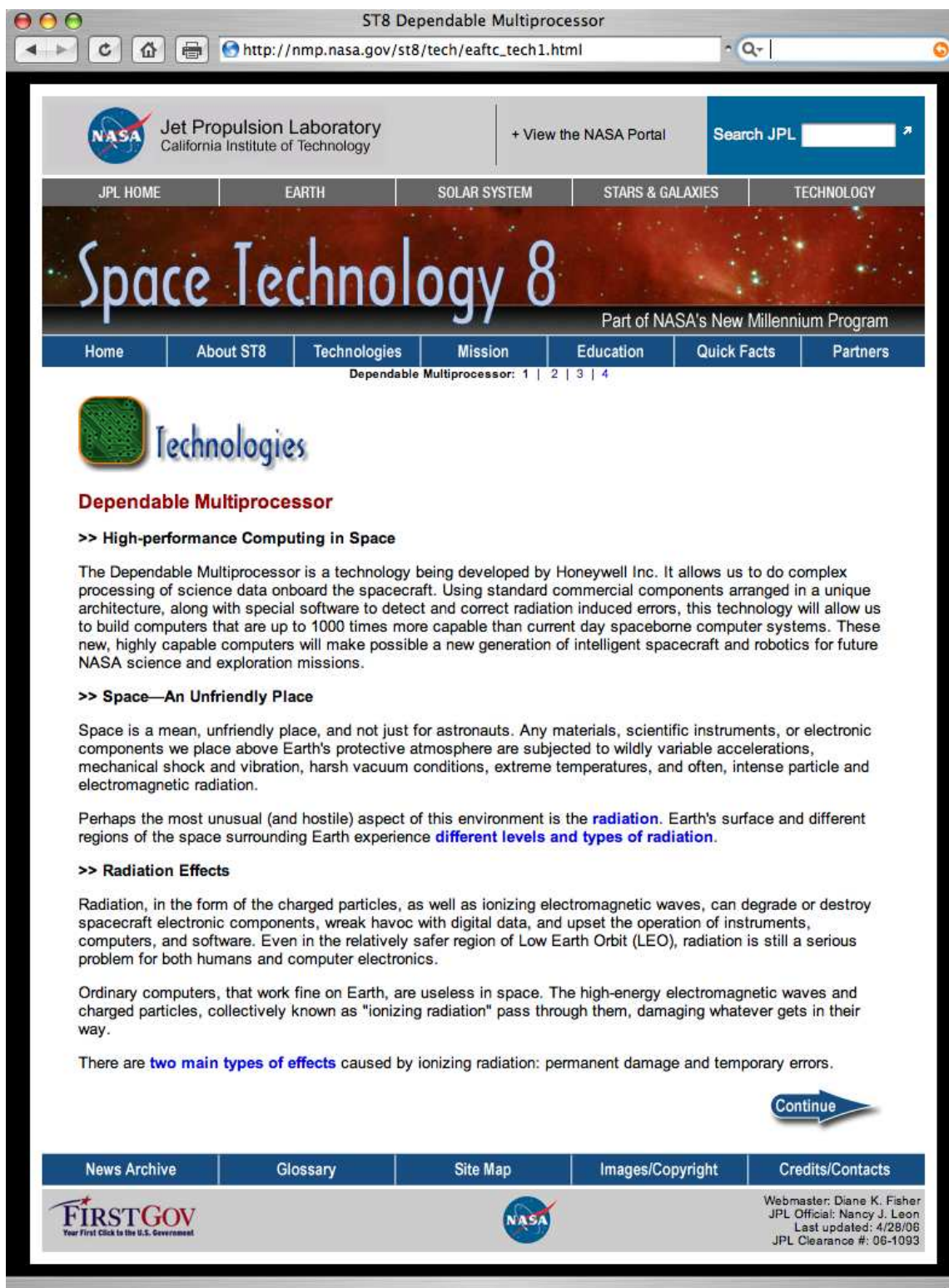
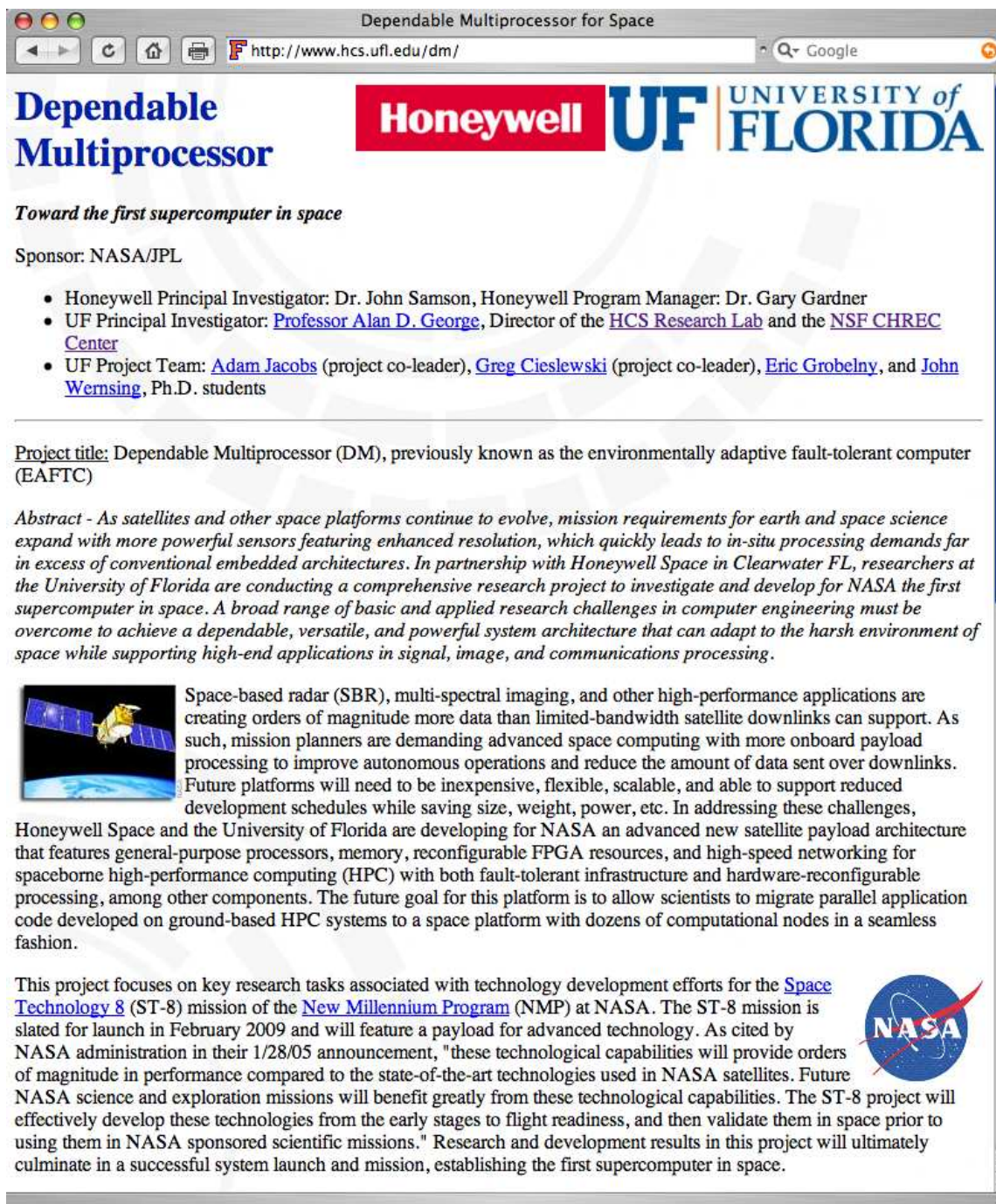


Figure 6: The New Millennium Program (NMP) Space Technology 8 (ST8) Dependable Multiprocessor (DM) project webpage at NASA's Jet Propulsion Laboratory.





Dependable Multiprocessor for Space

<http://www.hcs.ufl.edu/dm/>

# Dependable Multiprocessor

**Honeywell** **UF** **UNIVERSITY of FLORIDA**


*Toward the first supercomputer in space*

Sponsor: NASA/JPL

- Honeywell Principal Investigator: Dr. John Samson, Honeywell Program Manager: Dr. Gary Gardner
- UF Principal Investigator: [Professor Alan D. George](#), Director of the [HCS Research Lab](#) and the [NSF CHREC Center](#)
- UF Project Team: [Adam Jacobs](#) (project co-leader), [Greg Cieslewski](#) (project co-leader), [Eric Grobelny](#), and [John Wernsing](#), Ph.D. students

**Project title:** Dependable Multiprocessor (DM), previously known as the environmentally adaptive fault-tolerant computer (EAFTC)

**Abstract -** As satellites and other space platforms continue to evolve, mission requirements for earth and space science expand with more powerful sensors featuring enhanced resolution, which quickly leads to in-situ processing demands far in excess of conventional embedded architectures. In partnership with Honeywell Space in Clearwater FL, researchers at the University of Florida are conducting a comprehensive research project to investigate and develop for NASA the first supercomputer in space. A broad range of basic and applied research challenges in computer engineering must be overcome to achieve a dependable, versatile, and powerful system architecture that can adapt to the harsh environment of space while supporting high-end applications in signal, image, and communications processing.



Space-based radar (SBR), multi-spectral imaging, and other high-performance applications are creating orders of magnitude more data than limited-bandwidth satellite downlinks can support. As such, mission planners are demanding advanced space computing with more onboard payload processing to improve autonomous operations and reduce the amount of data sent over downlinks. Future platforms will need to be inexpensive, flexible, scalable, and able to support reduced development schedules while saving size, weight, power, etc. In addressing these challenges, Honeywell Space and the University of Florida are developing for NASA an advanced new satellite payload architecture that features general-purpose processors, memory, reconfigurable FPGA resources, and high-speed networking for spaceborne high-performance computing (HPC) with both fault-tolerant infrastructure and hardware-reconfigurable processing, among other components. The future goal for this platform is to allow scientists to migrate parallel application code developed on ground-based HPC systems to a space platform with dozens of computational nodes in a seamless fashion.

This project focuses on key research tasks associated with technology development efforts for the [Space Technology 8](#) (ST-8) mission of the [New Millennium Program](#) (NMP) at NASA. The ST-8 mission is slated for launch in February 2009 and will feature a payload for advanced technology. As cited by NASA administration in their 1/28/05 announcement, "these technological capabilities will provide orders of magnitude in performance compared to the state-of-the-art technologies used in NASA satellites. Future NASA science and exploration missions will benefit greatly from these technological capabilities. The ST-8 project will effectively develop these technologies from the early stages to flight readiness, and then validate them in space prior to using them in NASA sponsored scientific missions." Research and development results in this project will ultimately culminate in a successful system launch and mission, establishing the first supercomputer in space.




Figure 7: The Dependable Multiprocessor project webpage at the High-performance Computing and Simulation (HCS) Research Laboratory at the University of Florida at Gainesville, Florida.

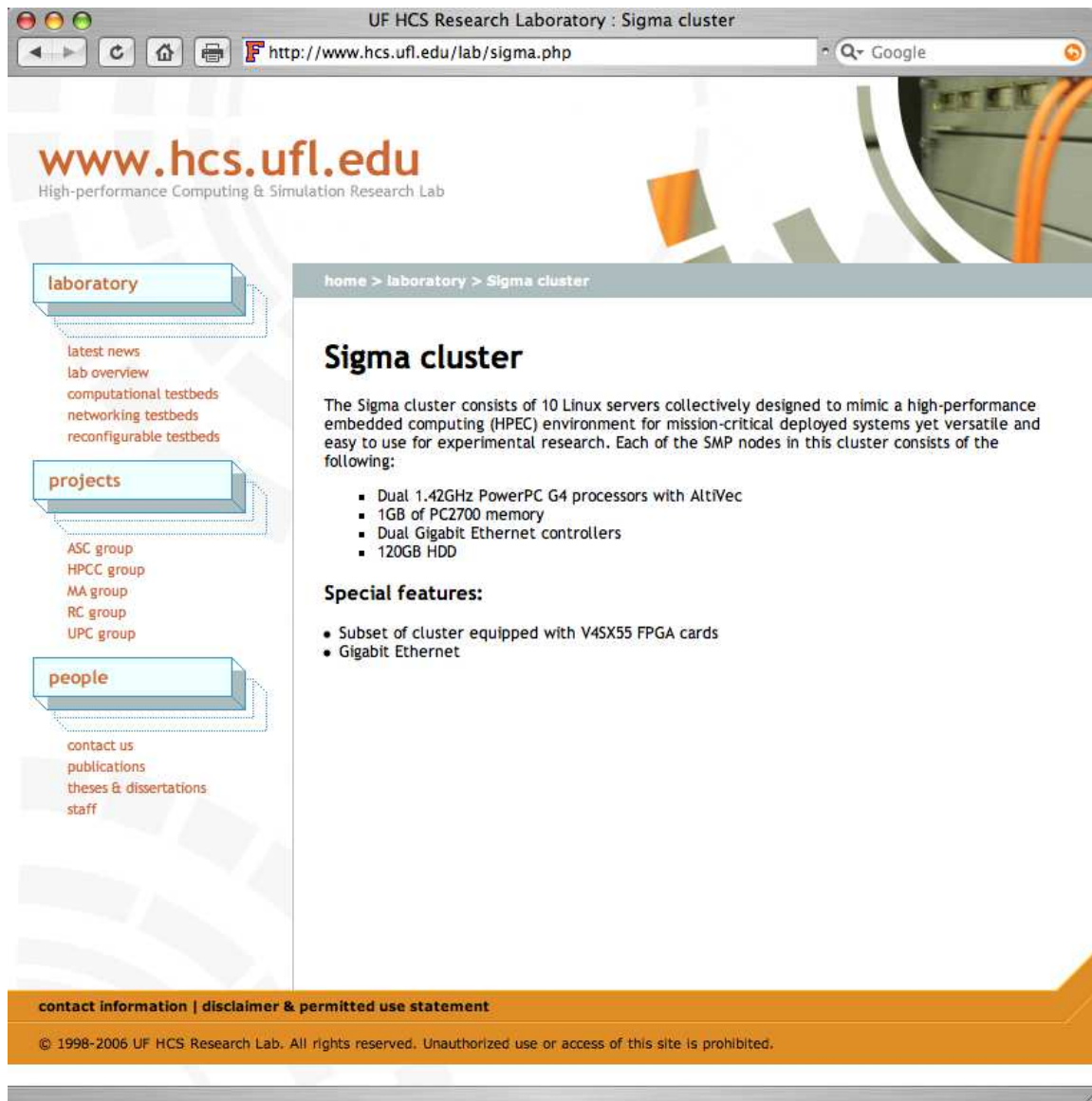


Figure 8: The HCS webpage describing the 10-node Linux cluster with 20 PowerPCs. This facility is used as a Dependable Multiprocessor software testbed.

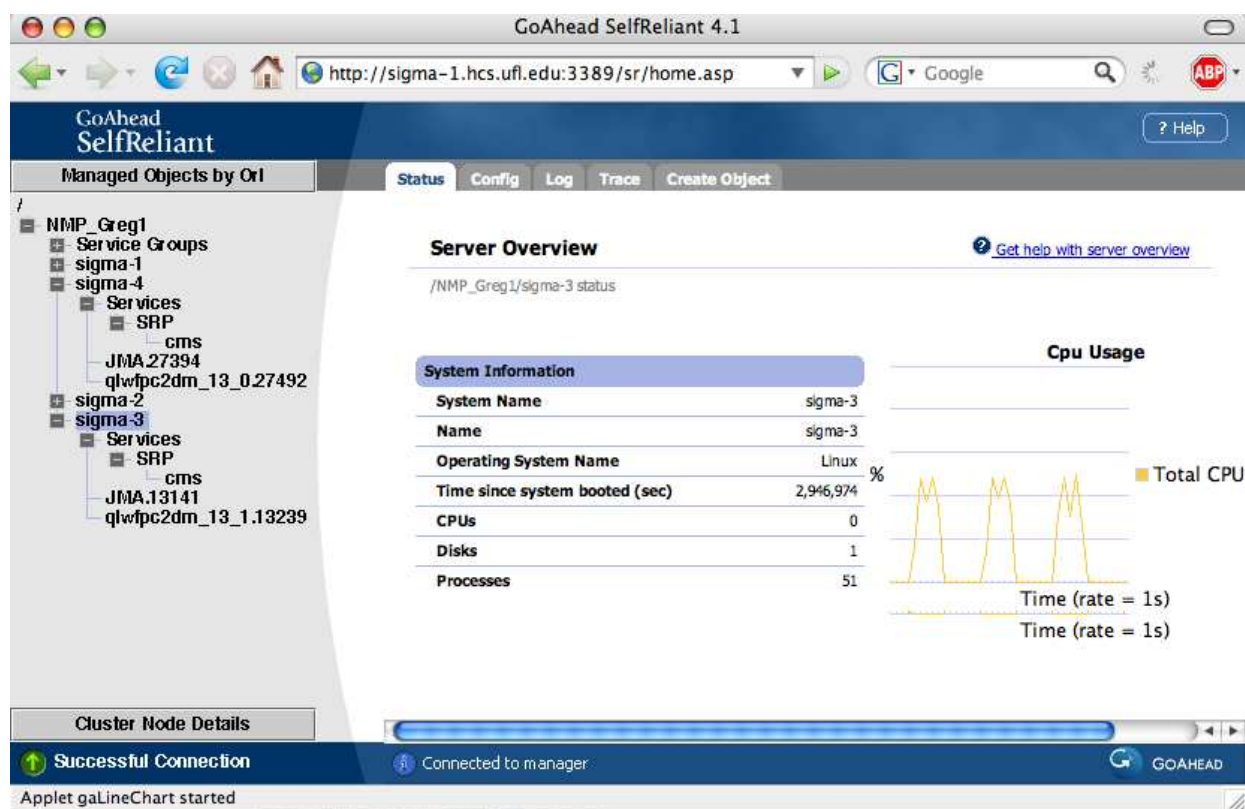


Figure 9: A snapshot of the GoAhead SelfReliant middleware cluster management webpage for the DM-sigma cluster showing the PI's QLWFPC2DM application running every 10 seconds on the sigma-3 compute node of the DM-sigma software-testbed cluster. A similar execution mode will be used during the software fault injection experiments that will begin in mid-March 2008.

**AISR-funded Publications from April 1, 2007 to March 30, 2008**

*The Lost Flux Method: A New Algorithm for Improving the Precision of Space-Based Near-Infrared Stellar Photometry with Lossy Detectors*, Mighell, K. J. 2007, ASP Conference Series: *Astronomical Data Analysis Software and Systems XVI*, edited by R. Shaw, F. Hill and D. Bell, 376, 405–408

*Improving the Precision of Near-Infrared Stellar Photometry by Modeling the Image Formation Process within a Lossy Detector*, Mighell, K. J. 2007, Proceedings of the 2007 NASA Science Technology Conference, held at the University of Maryland University College on June 19–21, 2007, 9 pages

[ [http://esto.nasa.gov/conferences/nstc2007/papers/Mighell\\_Kenneth\\_A6P3\\_NSTC-07-0016.pdf](http://esto.nasa.gov/conferences/nstc2007/papers/Mighell_Kenneth_A6P3_NSTC-07-0016.pdf) ]

*Enhancing the Science Return of the Spitzer Warm Mission*, Mighell, K. J. 2007, Proceedings of the 2007 Advanced Maui Optical and Space Surveillance Technologies Conference, held in Wailea, Maui, Hawaii, September 12–15, 2007, edited by S. Ryan, The Maui Economic Development Board, 301–312

*The Lost Flux Method: Improving the Precision of Space-Based Near-Infrared Stellar Photometry with Lossy Detectors*, Mighell, K. J. 2008 (submitted to ApJ on January 17, 2008)



## References

- [1] *Stellar Photometry and Astrometry with Discrete Point Spread Functions*,  
Mighell, K. J. 2005,  
MNRAS, 361, 861–878
- [2] *Infrared Array Camera Data Handbook (Version 3.0; January 20, 2006)*,  
Reach, W. T., et al. 2006  
[ <http://ssc.spitzer.caltech.edu/irac/dh/iracdatahandbook3.0.pdf> ]
- [3] *Improving the Precision of Near-Infrared Stellar Photometry by Modeling the Image Formation Process within a Lossy Detector*,  
Mighell, K. J. 2007,  
Proceedings of the 2007 NASA Science Technology Conference, held at the University of Maryland University College on June 19–21, 2007, 9 pages  
[ [http://esto.nasa.gov/conferences/nstc2007/papers/Mighell\\_Kenneth\\_A6P3\\_NSTC-07-0016.pdf](http://esto.nasa.gov/conferences/nstc2007/papers/Mighell_Kenneth_A6P3_NSTC-07-0016.pdf) ]
- [4] *Enhancing the Science Return of the Spitzer Warm Mission*,  
Mighell, K. J. 2007,  
Proceedings of the 2007 Advanced Maui Optical and Space Surveillance Technologies Conference, held in Wailea, Maui, Hawaii, September 12–15, 2007, edited by S. Ryan, The Maui Economic Development Board, 301–312
- [5] SPIE Symposium on Astronomical Instrumentation 2008 webpage:  
<http://spie.org/astronomical-instrumentation.xml>
- [6] van Dokkum, P. G. 2001, PASP, 113, 1420–1427
- [7] *Technology Validation: NMP ST8 Dependable Multiprocessor Project*,  
Samson, J., George, A., Gardner, G., Lupia, D., Some, R., Patel, M., Davis, P., &, Aggarwal, V., Kalbarczyk, Z.  
Proceedings of the 2007 NASA Science Technology Conference, held at the University of Maryland University College on June 19–21, 2007, 18 pages  
[ [http://esto.nasa.gov/conferences/nstc2007/papers/Samson\\_John\\_D1P4\\_NSTC-07-0047.pdf](http://esto.nasa.gov/conferences/nstc2007/papers/Samson_John_D1P4_NSTC-07-0047.pdf) ]
- [8] *Technology Readiness Levels: A White Paper*,  
Mankins, J. C. 1995,  
Advanced Concepts Office, Office of Space Access and Technology, NASA (April 6, 1995)  
[ <http://www.hq.nasa.gov/office/codeq/tr1/tr1.pdf> ]
- [9] *QLWFPC2: Parallel-Processing Quick-Look WFPC2 Stellar Photometry Based on the Message Passing Interface*,  
Mighell, K. J. 2004,  
ASP Conference Series: Astronomical Data Analysis Software and Systems XIII,  
edited by F. Ochsenbein, M.-G. Allen, and D. Egret, 314, 678–681
- [10] *The Lost Flux Method: A New Algorithm for Improving the Precision of Space-Based Near-Infrared Stellar Photometry with Lossy Detectors*,  
Mighell, K. J. 2007,  
ASP Conference Series: Astronomical Data Analysis Software and Systems XVI,  
edited by R. Shaw, F. Hill and D. Bell, 376, 405–408

# Improving the Precision of Near-Infrared Stellar Photometry by Modeling the Image Formation Process within a Lossy Detector

Kenneth Mighell

National Optical Astronomy Observatory  
950 North Cherry Avenue  
Tucson, AZ 85719 U.S.A.

**Abstract**—A detector can be considered to be effectively lossy if a pixel, the smallest optically sensitive unit of the detector, internally exhibits a non-uniform response function that has a quantum efficiency variation with an rms dispersion exceeding an arbitrary level of 1%. Near-infrared astronomical cameras based on lossy detectors can have large systematic errors in the measurement of total stellar flux if stellar images are undersampled. While this problem can be mitigated by oversampling the stellar image, many near-infrared cameras are deliberately undersampled in order to achieve a large field of view. The combination of undersampling stellar images on lossy detectors is currently diminishing the potential science return of some of the near-infrared cameras onboard the *Hubble Space Telescope* and the *Spitzer Space Telescope*. Although the recorded stellar flux can be corrupted by using detectors with significant effective intrapixel quantum efficiency variations, it is still possible to achieve excellent stellar photometry – if the image formation process inside the detector is accurately modeled. During the past year, I have worked with *Spitzer Space Telescope*’s Infrared Array Camera (IRAC) Instrument Team to demonstrate that my NASA-funded MATPHOT algorithm for precision stellar photometry and astrometry using discrete Point Spread Functions can yield an improvement in the precision of bright star stellar photometry, obtained from IRAC Ch1 observations, of more than 100% over the best results obtained with aperture photometry using the recommended calibration procedures in the IRAC Data Handbook. This collaborative effort will continue with the goal of developing new calibration procedures for that have the potential of significantly improving the precision of IRAC point-source photometry. This effort is timely because IRAC Ch1 and Ch2 will be the only operational cameras available during the *Spitzer* Warm Mission which is nominally scheduled to start about April 2009 after all of the cryogen has been depleted. This work was supported by grants from the Applied Information Systems Research (AISR) Program of NASA’s Science Mission Directorate.

## I. INTRODUCTION

Current near-infrared detector technology can produce space-based astronomical imagers with non-uniform pixel response functions. Large intrapixel quantum efficiency (QE) variations can cause significant loss of stellar flux depending on where a star is centered within the central pixel of the stellar image. Reference [1] measured a peak-to-peak variation of 0.39 mag at the *J* band (F110W) and 0.22 mag at *H* band (F160W) of the NIC3 camera of the *Hubble Space Telescope* (HST) NICMOS instrument [2], [3]. The peak-to-peak variation of  $\sim 0.2$  mag at F160W with NIC3 has been independently

verified [4]. Significant flux loss due to non-uniform intrapixel response functions is clearly an observational fact in some existing space-based near-infrared astronomical cameras.

Even existing NASA-grade optical CCDs (charge coupled devices) can have minor intrapixel QE variations across a single pixel. Reference [1] found that the *V*-band (F555W) Point Spread Function (PSF) of the WFC (Wide Field Camera) of the *HST* WFPC2 instrument [5], [6] has a peak-to-peak range of 0.030 mag and an rms dispersion of 0.008 mag; the effect at the *I* band (F814W) is slightly better with a peak-to-peak error range of 0.023 mag with a 0.006 mag dispersion. This small but measurable variation of the quantum efficiency within a WFC pixel is a contributing factor to the minimum image-to-image photometric scatter of 0.01 mag that has been found in dithered WFPC2 stellar observations (see, e.g., [7]–[12]).

NASA (National Aeronautics and Space Administration) and ESA (European Space Agency) astrophysical mission managers have a penchant for approving of camera designs which use undersampled detectors on the focal plane in order to achieve a wider field of view. Unfortunately, the analysis of image data from cameras with undersampled detectors is frequently problematical. Analysis difficulties are further compounded when the detectors used in such cameras are lossy.

A detector can be considered to be effectively lossy if a pixel, the smallest optically sensitive unit of the detector, internally exhibits a non-uniform response function that has a quantum efficiency variation with an rms dispersion exceeding an arbitrary level of 1%. By this user-centric definition, the detectors in NIC3 camera of the NICMOS instrument are lossy but the detectors used in the WFC cameras of the WFPC2 instrument are not.

This article describes how the precision of stellar photometry from an existing space-based near-infrared camera with a lossy detector can be significantly improved by compensating the apparent loss of stellar flux through modeling of the image formation process within the detector. Section II describes the role of Point Response Functions in the image formation process. A photometric and astrometric performance model for CCD stellar observations is given in Section III. The key features of the MATPHOT algorithm for precision stellar pho-

tometry and astrometry with discrete (sampled) Point Spread Functions are briefly outlined in Section IV. Observations of a bright star obtained with Channel 1 of the *Spitzer Space Telescope* Infrared Array Camera (IRAC) instrument are described in Section V and analyzed using aperture photometry in Section VI and then MATPHOT photometry in Section VII. Concluding remarks are given in Section VIII.

## II. POINT RESPONSE FUNCTIONS

A Point Response Function (PRF),  $\Psi$ , of an astronomical imaging system with a detector is the convolution of a Point Spread Function (PSF),  $\phi$ , and a Detector Response Function (DRF),  $\Lambda$  :

$$\Psi \equiv \phi * \Lambda . \quad (1)$$

The PSF describes the two-dimensional distribution of photons from a star *just above the detector*. Although stellar photons are distributed as a point source above the Earth's atmosphere, a stellar image becomes a two-dimensional distribution as the stellar photons are scattered by atmospheric turbulence. The blurred stellar image is then further degraded by passage of the stellar photons through the combined telescope and camera optical elements (such as mirrors, lenses, apertures, etc.). The PSF is the convolution of all these blurring effects on the original stellar point source.

The DRF is a two-dimensional discrete (sampled) function that describes how the detector electronics convert stellar photons ( $\gamma$ ) to electrons ( $e^-$ ) — including such effects as the diffusion of electrons within the detector substrate or the reflection (absorption) of photons on (in) the gate structures of the detector electronics. A perfect DRF gives a PRF that is a *sampled version* of the PSF:

$$\Psi_i \equiv \int_{x_i-0.5}^{x_i+0.5} \int_{y_i-0.5}^{y_i+0.5} \phi(x, y) dx dy , \quad (2)$$

where  $i^{\text{th}}$  pixel (px) of the PRF located at  $(x_i, y_i)$  is the volume integral of the PSF over the area of the  $i^{\text{th}}$  pixel. The actual limits of the above volume integral reflect the appropriate mapping transformation of the  $x$  and  $y$  coordinates onto the CCD pixel coordinate system.

The volume,  $V$ , of a PRF is, by definition, one or less:

$$V \equiv \iint (\phi * \Lambda) dx dy \equiv \sum_i \Psi_i \leq 1 , \quad (3)$$

where the integration and summation are over all pixels which are illuminated by the PSF. A PRF volume that is less than one indicates that a loss of stellar photons has occurred during the detection/conversion process within the detector.

The effective-background area,  $\beta$ , of a PRF is defined as the reciprocal of the summation of the square of the PRF:

$$\beta \equiv \frac{1}{\sum_i \Psi_i^2} . \quad (4)$$

Physically,  $\beta$  can be thought of as the noise “footprint” (in pixels) of a stellar image on the sky. The effective-background

area is an observing-efficiency metric (small  $\beta$  values are better) that is used to make accurate predictions of the photometric and astrometric performance limits of stellar observations obtained with state-of-the-art astrophysical imagers with lossy detectors; this metric measures the combination of camera focus and detector efficiency: for any given detector, the smallest  $\beta$  values are obtained when the camera is focused and, similarly, for any given focus, the smallest  $\beta$  values are obtained when the efficiency of the detector is maximized [13].

The  $S_1$  image sharpness parameter from the seminal paper of Muller & Buffington [14] is the summation of the square of the normalized PRF:

$$S_1 \equiv \sum_i \tilde{\Psi}_i^2 \equiv \sum_i \left( \frac{\Psi_i}{V} \right)^2 \equiv \text{sharpness} . \quad (5)$$

Physically,  $S_1$  is a shape parameter that describes the “pointiness” of a PRF;  $S_1$  values range from a maximum of one (all of the stellar flux is found within a single pixel) to a minimum of zero (a flat stellar image). For example, cameras that are out of focus have broad PSFs with  $S_1$  values near zero. A normalized Gaussian [15] PSF with a standard deviation of  $\sigma$  pixels that has been *oversampled* with a perfect DRF (where  $V=1$ ) will have a  $S_1$  value of  $1/4\pi\sigma^2$ . A *critically-sampled* normalized Gaussian PRF (where  $\sigma \equiv 1$ ) thus has a  $S_1$  value of  $1/(4\pi)$  and any PRF with a  $S_1$  value greater than that value ( $\sim 0.0796$ ) can be described as being undersampled. The  $S_1$  image sharpness parameter has proven to be such a useful image quality metric that one finds references to it in the astrophysical literature where it is simply called sharpness without citing Muller & Buffington (see, e.g., Section 6.5.1 of [6] and Section 2.1 of [13]).

Diffraction limited optics, theoretically, give  $S_1$  values that decrease (i.e., PSFs become flatter) with increasing photon wavelength — for a fixed pixel (detector) size. With real astronomical cameras, observed  $S_1$  values frequently depend on *where the center of a star is located within the central CCD pixel* of the stellar image. For example, the *HST* WFPC2 Planetary Camera PRF at a wavelength of 200 nm has an observed  $S_1$  value of 0.084 if the PRF is centered in the middle of a PC pixel or 0.063 if the PRF is centered on a pixel corner (see Table 6.5 of [6]); at 600 nm the observed  $S_1$  values range from 0.066 (pixel-centered) to 0.054 (corner-centered). The Wide-Field Cameras of the *HST* WFPC2 instrument have pixels which are approximately half the angular resolution of the PC camera pixels; WFC stellar images are undersampled and the observed range of  $S_1$  values are 0.102–0.120 at 200 nm and 0.098–0.128 at 600 nm.

The *normalized* effective-background area,  $\tilde{\beta}$ , of a PRF is defined as the reciprocal of the summation of the square of the normalized PRF; it is a focus metric which has an optimal (minimum) value when a camera is in focus. The normalized effective-background area of a PRF, also called NoisePixels by the IRAC Instrument Team (see, e.g., [16]–[19]), is equivalent

to the inverse of the  $S_1$  image sharpness parameter:

$$\tilde{\beta} \equiv \frac{1}{\sum_i \tilde{\Psi}_i^2} \equiv \beta V^2 \equiv \frac{1}{S_1} \equiv \text{NoisePixels}. \quad (6)$$

A critically-sampled Gaussian PSF has a normalized effective-background area value of  $4\pi$  ( $\approx 12.57$ ) px; any PRF can be considered to be undersampled if  $\tilde{\beta} < 4\pi$ . Numerical integration of a realistic ground-based stellar profile gives a normalized effective-background area of  $30.8 \sigma^2$  instead of the value of  $4\pi \sigma^2$  for a Gaussian profile with a standard deviation of  $\sigma$  pixels [20].

### III. PERFORMANCE MODEL

Consider a CCD observation of single isolated star on a flat sky background. Assuming one already knows the PRF of the observation at the location of the star, a simple model of the observation would have just two parameters: the stellar intensity ( $\mathcal{E}$ ) in electrons, and the observed background sky level ( $\mathcal{B}$ ) in electrons. The observational model for the  $i^{\text{th}}$  pixel would be

$$m_i \equiv \mathcal{B} + \mathcal{E} V \tilde{\Psi}_i, \quad (7)$$

where  $V$  is the volume integral of the PRF and  $\tilde{\Psi}_i$  is the value of the  $i^{\text{th}}$  pixel of the *normalized* PRF ( $\tilde{\Psi}_i \equiv \Psi_i/V$ ).

The *upper limit* for the photometric signal-to-noise ratio (S/N) of a CCD observation of a single isolated star on a flat sky can be estimated as follows:

$$\begin{aligned} \text{S/N} &\equiv \frac{\mathcal{E}}{\sigma_{\mathcal{E}}} \\ &\approx \frac{\mathcal{E}}{\sqrt{\frac{\mathcal{E}}{V} + \beta \left(1 + \sqrt{\beta/N}\right)^2 \sigma_{\text{rms}}^2}} \end{aligned} \quad (8)$$

$$\approx \frac{\mathcal{E}}{\sqrt{\frac{\mathcal{E}}{V} + \beta \left(1 + \sqrt{\beta/N}\right)^2 [\mathcal{B} + \sigma_{\text{RON}}^2]}} \quad (9)$$

where

$$\sigma_{\text{rms}} \equiv \sqrt{\frac{1}{N} \sum_{i=1}^N \sigma_i^2} \approx \sqrt{\mathcal{B} + \sigma_{\text{RON}}^2}, \quad (10)$$

$N$  is the number of pixels in the observation,  $\sigma_i$  is the measurement error (one standard deviation) of the  $i^{\text{th}}$  pixel, the background sky is assumed to be a Poisson distribution with a mean of  $\mathcal{B}$  electrons, and  $\sigma_{\text{RON}}$  is the rms readout noise [13]. These approximations assume, for the sake of simplicity, that any noise contribution due to dark current and quantization noise is negligible. While these additional noise sources can be added to create an even more realistic performance model for stellar photometry, the assumption of low dark current and minimal quantization noise is realistic for state-of-the-art astronomical-grade CCD imagers. The resulting photometric error is approximately

$$\Delta \text{mag} \approx \frac{1.0857}{\text{S/N}}, \quad (11)$$

where the constant 1.0857 is an approximation for Pogson's ratio  $a \equiv 5/\ln(100) = 2.5 \log(e)$  [21].

The *lower limit* of the rms measurement error for the stellar  $\mathcal{X}$  position of a CCD observation of a single isolated star on a flat sky can be estimated as follows:

$$\sigma_{\mathcal{X}} \approx \sqrt{\frac{\mathcal{L}^2}{\mathcal{E}V} \left[1 + 8\pi \sigma_{\text{rms}}^2 \frac{\mathcal{L}^2}{\mathcal{E}V}\right]} \quad (12)$$

$$\approx \sqrt{\frac{\mathcal{L}^2}{\mathcal{E}V} \left[1 + 8\pi (\mathcal{B} + \sigma_{\text{RON}}^2) \frac{\mathcal{L}^2}{\mathcal{E}V}\right]} \quad (13)$$

where

$$\mathcal{L} \equiv \sqrt{\frac{\tilde{\beta}}{4\pi}} = \frac{1}{\sqrt{4\pi S_1}} \quad (14)$$

is the *critical-sampling scale length* of the PRF in pixel units (px) [13]. By definition, the critical-sampling scale length of a critically-sampled PRF imaged with a perfect detector is one pixel;  $\mathcal{L} > 1$  indicates that the PRF is *oversampled*, while  $\mathcal{L} < 1$  indicates that the PRF is *undersampled*.

The *lower limit* of the rms measurement error for the stellar  $\mathcal{Y}$  position of a CCD observation of a single isolated star on a flat sky can be estimated, by symmetry, as follows:

$$\sigma_{\mathcal{Y}} = \sigma_{\mathcal{X}}. \quad (15)$$

### IV. MATPHOT ALGORITHM

The MATPHOT algorithm for precise and accurate stellar photometry and astrometry with discrete PSFs was described in detail in reference [13]. The current C-language [22] implementation of the MATPHOT algorithm works with user-provided discrete (sampled) PSFs consisting of a numerical table represented by a matrix in the form of a FITS image [23]. Position partial derivatives are computed [24] using the following five-point numerical differentiation formula,

$$\begin{aligned} f'(x_i) &\approx \frac{1}{12} [f(x_{i-2}) - 8f(x_{i-1}) + 8f(x_{i+1}) - f(x_{i+2})], \end{aligned} \quad (16)$$

from [25], and discrete PSFs are shifted [26] within an observational model using the following 21-pixel-wide damped sinc function,

$$\begin{aligned} f^{\text{shifted}}(x_0) &\equiv \sum_{i=-10}^{10} f(x_i) \frac{\sin(\pi(x_i - x_0))}{\pi(x_i - x_0)} \exp\left(-\left[\frac{x_i - x_0}{3.25}\right]^2\right), \end{aligned} \quad (17)$$

from the ZODIAC C library written by Marc Buie of Lowell Observatory, which was specifically designed for use with 32-bit floating numbers. Precise and accurate stellar photometry and astrometry are achieved with undersampled CCD observations by using supersampled discrete PSFs that are sampled 2, 3, or more times more finely than the observational data. Although these numerical techniques are not mathematically



perfect, they are sufficiently accurate for precision stellar photometry and astrometry due to photon noise which is present in all astronomical imaging observations. The current photometric reduction code<sup>1</sup> is based on a robust implementation of the Levenberg-Marquardt method of nonlinear least-squares minimization [27]–[30]. Detailed analysis of simulated *Next Generation Space Telescope* (NGST) observations demonstrate that millipixel relative astrometry and millimag photometric precision should be achievable with complicated space-based discrete PSFs [13]. The MATPHOT algorithm achieves the theoretical performance expectations [13] for accurate and precise stellar photometry and astrometry described in the previous section.

## V. OBSERVATIONS

I analyzed 16 short (0.6 s) frames<sup>2</sup> from a focus check calibration on the K0-class star PPM 9412 (a.k.a. HIP 6378) from Channel 1 (3.6  $\mu\text{m}$ ) of the Infrared Array Camera (IRAC) [19] onboard the *Spitzer Space Telescope*. The observation was on 2003 October 8 UT, after all focus adjustments had been completed. The locations of the star on the array were distributed roughly evenly across a 4x4 pixel box near the array center. The IRAC basic calibrated data (BCD) images were retrieved from the *Spitzer* data archive with the kind assistance of IRAC Instrument Team member Bill Glaccum.

## VI. APERTURE PHOTOMETRY

Square aperture photometry with a 21 $\times$ 21 pixel box centered on a star was performed using the interactive “m” keyboard command of the *imexamine* task of the IRAF data reduction and analysis system [31], [32]. A 5.6% peak-to-peak spread was seen in these square aperture flux measurements (see Fig. 1). *A nonrandom variation in flux is quite apparent in these 16 IRAC Ch1 observations:* the total stellar flux measured is strongly correlated with the amount of flux found in the central pixel (see Fig. 2).

Examination of the individual observations revealed that the observations with the most stellar flux have stellar images that are centered in the middle of a pixel while those observations with the least stellar flux are centered on a pixel corner. This effect, shown graphically in Fig. 3 (which is Fig. 5.1 of the IRAC Data Handbook [33]), is due to the combination of large quantum efficiency variations within individual pixels and the undersampling of the Point Spread Function (PSF) by the Detector Response Function (DRF). The loss flux is most severe in Channel 1 (3.6  $\mu\text{m}$ ) where the correction can be as much as 4% peak to peak [33].

<sup>1</sup>All source code and documentation for MATPHOT and support software are freely available at NOAO: <http://www.noao.edu/staff/mighell/matphot>

<sup>2</sup>Observations: ads/sa.spitzer#00068nnnnn where nnnnn is 75392, 76672, 76928, 77184, 77440, 77696, 77952, 78208, 78464, 78720, 78976, 79232, 79488, 79744, 80000, 80256.

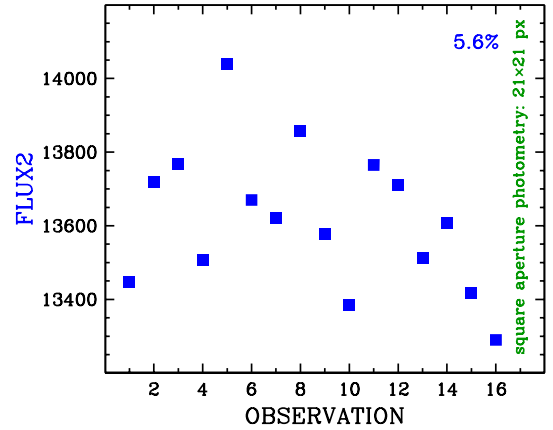


Fig. 1. Square aperture photometry of IRAC Ch1 observations of a single bright star.

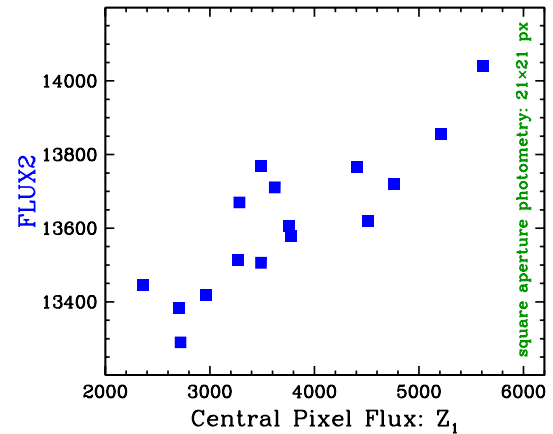


Fig. 2. Same data as in Fig. 1 but sorted by the flux value of the central pixel of the stellar image.

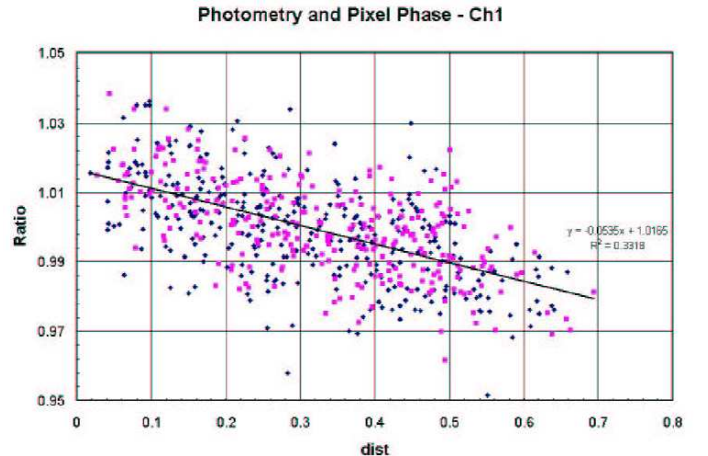


Fig. 3. **Figure 5.1 of the IRAC Data Handbook** [33]. Dependence of point source photometry on the distance of the centroid of a point source from the nearest pixel center in channel 1. The ratio on the vertical axis is the measured flux density to the mean value for the star, and the quantity on the horizontal axis is the fractional distance of the centroid from the nearest pixel center.

This is the relevant extract from the IRAC Data Handbook [33]:

The flux density of a point source measured from IRAC images depends on the exact location where the peak of the Point Response Function (PRF) falls on a pixel. This effect is due to the variations in the quantum efficiency of a pixel, and combined with the undersampling of the PRF, it is most severe in channel 1. The correction can be as much as 4% peak to peak. The effect is graphically shown in Figure 5.1 (see Fig. 3 of this article) where the normalized measured flux density (y-axis) is plotted against the distance of the source centroid from the center of a pixel. The correction for channel 1 can be calculated from

$$Correction = 1 + 0.0535 \times \left[ \frac{1}{\sqrt{2\pi}} - p \right] \quad (5.14)$$

where  $p$  is the pixel phase ( $p = \sqrt{(x-x_0)^2 + (y-y_0)^2}$ ), where  $x, y$ , is the centroid of the point source and  $x_0$  and  $y_0$  are the integer pixel numbers containing the source centroid. The correction was derived from photometry of a sample of stars, each star observed at many positions on the array. The “ratio” on the vertical axis in Figure 5.1 is the ratio of the measured flux density to the mean value for the star. To correct the flux of a point source, calculate the correction from Equation 5.14 and divide the source flux by that correction. Thus, the flux of sources well-centered in a pixel will be reduced by 2.1%. Pixel phase corrections for other channels, if necessary, and after they have been more accurately determined than currently, will be given in future Data Handbook versions.

The application of the recommended radial flux correction requires an accurate estimate of the position of the center of the star. IRAF’s *imexamine* task can produce accurate centroid estimates for circular aperture photometry but not for square aperture photometry. So in order to apply the radial flux correction recommended by the IRAC Data Handbook, circular aperture photometry was performed on the observations shown in Fig. 1.

Circular aperture photometry centered on the star with a radius of 10 pixels (px) was done using the interactive “a” keyboard command of the *imexamine* task of IRAF. A **5.3%** peak-to-peak spread was found in the raw circular aperture flux measurements (see Fig. 4: open circles). Applying the recommended Ch1 flux correction from the IRAC Data Handbook only slightly reduced the peak-to-peak spread to **4.9%** (see Fig. 4: filled circles).

Reducing the aperture radius to just 5 pixels does improve the photometric precision; a **4.5%** peak-to-peak spread was found in the raw circular aperture flux measurements (see Fig. 5: open circles) which reduced to **3.5%** when the recommended Ch1 flux correction was applied (see Fig. 5: filled circles). *This is the best that aperture photometry can do with the recommended radial correction.*

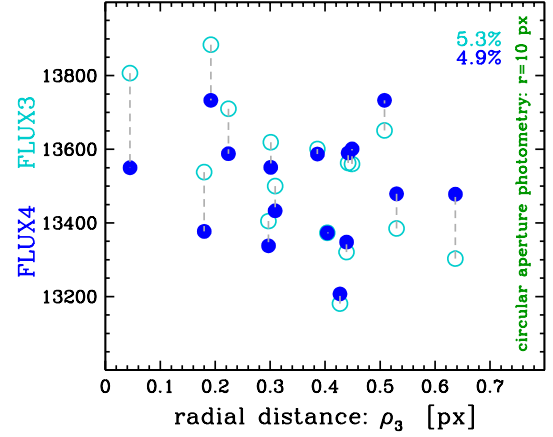


Fig. 4. Circular aperture photometry with a radius of 10 pixels of the observations shown in Fig. 1. The filled (open) circles show the corrected (raw) flux values.

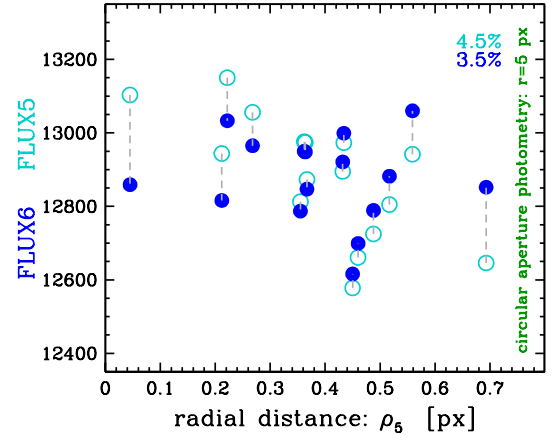


Fig. 5. Circular aperture photometry with a radius of 5 pixels. The filled (open) circles show the corrected (raw) flux values.

## VII. MATPHOT PHOTOMETRY

IRAC Ch1 PSFs are significantly undersampled by the IRAC Ch1 camera [19]. A theoretical  $5 \times 5$  supersampled version of the IRAC PSF for the central region of Ch1 is shown in Fig. 6 [34]. Although the PSF appears to be reasonable in the linear stretch (*left graph*), which emphasizes the bright central core, the log stretch (*right graph*) shows the numerous weak higher-spatial-frequency features of this very complicated PSF.

Bill Hoffmann, an IRAC Instrument Team member at the University of Arizona, made the first estimate [35] of the intrapixel quantum efficiency variation across a single IRAC Ch1 pixel:

$$\text{intrapix} = \begin{pmatrix} 0.813 & 0.875 & 0.875 & 0.875 & 0.813 \\ 0.875 & 1.000 & 1.000 & 1.000 & 0.875 \\ 0.875 & 1.000 & 1.000 & 1.000 & 0.875 \\ 0.875 & 1.000 & 1.000 & 1.000 & 0.875 \\ 0.813 & 0.875 & 0.875 & 0.875 & 0.813 \end{pmatrix}.$$

Each element is the mean RQE (relative quantum efficiency) value, relative to the center of the pixel, over a  $0.2 \times 0.2$  pixel<sup>2</sup>

area. Such a variation in QE across a pixel could be obtained if photogenerated charges originating at a pixel edge are more likely to recombine than charges originating near a pixel center, because they must random walk further before being collected. The QE variation is expected to be symmetrical about the center of a pixel, since the InSb layer is opaque over the bandpasses of Channels 1 and 2.

An experimental version of the MATPHOT stellar photometry code, called MPDZ, was developed to simulate and analyze IRAC Ch1 observations [36]–[39]. MPDZ models the image formation process within IRAC Ch1 by convolving the  $5 \times 5$  supersampled theoretical PSF for the central region of IRAC Ch1 PSF shown in Fig. 6 with the above relative intrapixel quantum efficiency (QE) variation map for IRAC Ch1.

Ten thousand IRAC Ch1 observations of a single star on a flat background were simulated and analyzed with MPDZ. Each stellar observation was simulated using the PSF shown above; a star with an intensity of  $10^6$  electrons was located near the center of an field of  $60 \times 60$  pixels on a flat background of 100 electrons.

The horizontal axis of Fig. 7 shows the subpixel offset (radial distance) the center of a star is from the middle of the central pixel; stars centered near the middle of a pixel will have small offset values while stars located near the corner of a pixel will have offsets near 0.7 px. The vertical axis of Fig. 7 shows the absolute flux ratio of the total fluxes divided by the true flux of  $10^6$  electrons. The light-grey points show the observed (raw) absolute flux ratios and the dark points show the *measured* absolute flux ratios as reported by MPDZ. Note that while the average stellar observation suffered an absolute flux loss of about 9%, stars centered near the middle of a pixel suffered, on average, an absolute flux loss of about 7% as compared to an absolute flux loss of about 11% for stars centered near a pixel corner. It is important to note that the vertical scatter seen in the observed flux ratios is not random but systematic; *a simple radial correction function can only partially recover the lost flux*. The measured absolute flux ratios are clustered around unity and are not a function of subpixel offset; the vertical scatter seen in the measured absolute flux ratios is random. This experiment shows that by modeling the image formation process within the detector, MPDZ was able to fully recover all of the stellar flux lost due to the non-uniform IRAC Ch1 intrapixel quantum efficiency variations.

The vertical axis of Fig. 8 shows the observed (raw) total flux divided by the median observed total flux value of all ten thousand stars. The median values of the box-and-whisker plots (the central horizontal bar in each box) range from an excess flux of about 2% for stars centered near the center of a pixel to a flux deficit of about 2% for stars centered near the corner of a pixel. *One sees that even after the recommended flux correction (thick line of right graph of Fig. 8) is applied, an approximate 3% peak-to-peak spread remains for many observations — this explains almost all of the 3.5% spread seen in the right graph of Fig. 5!*

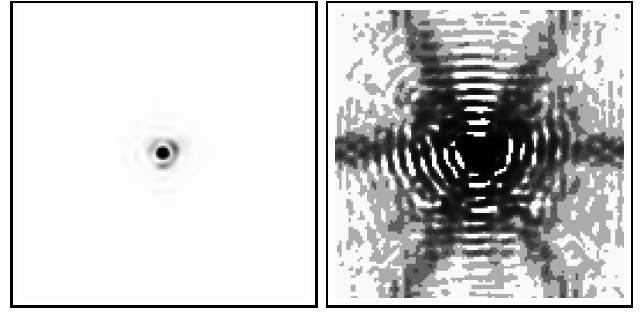


Fig. 6. A theoretical  $5 \times 5$  supersampled model of the IRAC PSF for the central region of Ch1. The left (right) graph shows a linear (log) stretch; black is high and white is low. Note the the numerous weak higher-spatial-frequency features of this very complicated PSF.

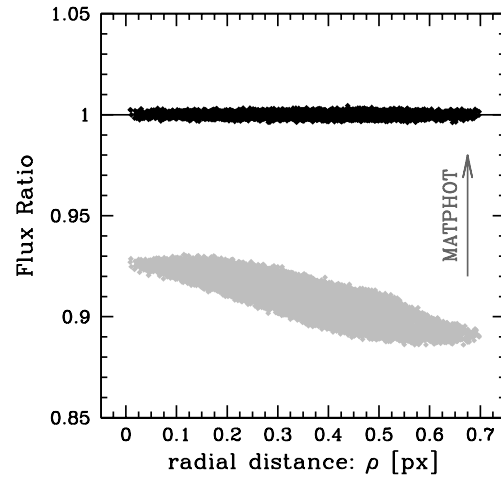


Fig. 7. MATPHOT analysis of 10,000 *simulated* IRAC Ch1 observations: observed (lower) versus measured (upper) flux ratios.

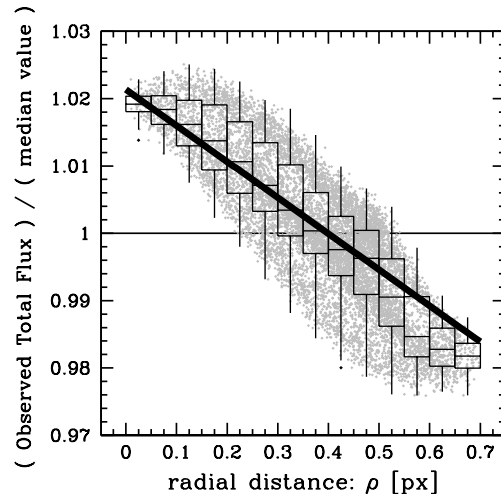


Fig. 8. MATPHOT analysis of 10,000 *simulated* IRAC Ch1 observations: *relative* observed flux ratios compared with the recommended radial flux correction (thick line) from the IRAC Data Handbook. Note how this figure reproduces almost exactly the observed flux loss distribution seen in Fig. 5.1 of the IRAC Data Handbook [33].

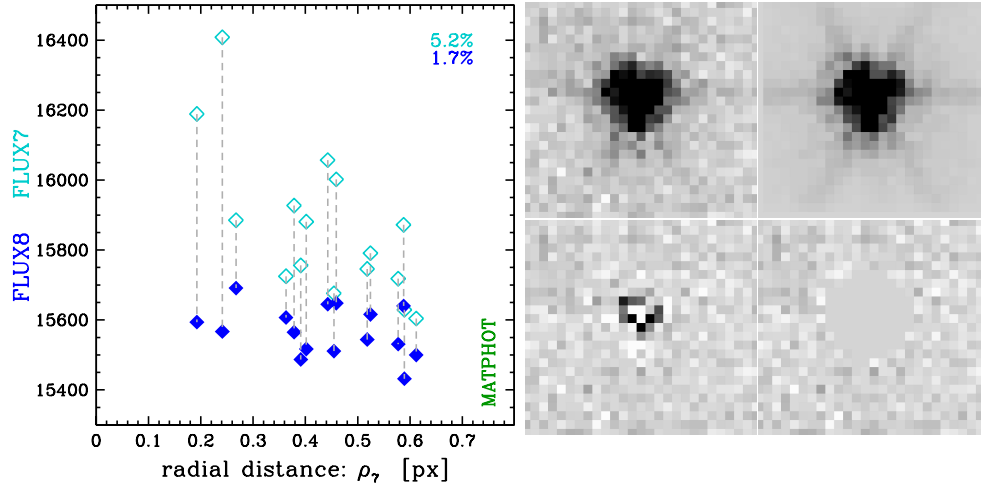


Fig. 9. MATPHOT observations of the observations shown in Fig. 1.

MATPHOT PSF-fitting photometry was performed on all of the observations using MPDZ with the theoretical  $5 \times 5$  supersampled IRAC Ch1 PSF shown in Fig. 6. The open diamonds in Fig. 6 show a **5.2%** peak-to-peak spread in the raw measured stellar flux values reported by MPDZ. The upper-left image in Fig. 9 shows central portion of the first IRAC Ch1 observation. The noiseless best-fit model of the observation is shown in the upper-right image. The residuals remaining after the best-fit model is subtracted from the observation are shown in the lower-left image. The lower-right image is the same as the residual image except that all residuals within a radius of 5 pixels from the fitted center of the star have been set to zero. All of these images are displayed with the same negative linear stretch which was chosen to emphasize the faint features of the stellar image. *The filled diamonds in Fig. 9 show a 1.7% peak-to-peak spread*; these flux values are the combination of the raw measured stellar fluxes (open diamonds) with the sum of all of residuals (positive and negative) within a radius of 5 pixels from the fitted center of the star.

MATPHOT with residuals (a.k.a. *The Lost Flux Method* [38], [39]) yields an improvement in photometric precision of more than 100% over the best results obtained with aperture photometry with the recommended radial correction: from **3.5%** peak-to-peak down to **1.7%**. Fig. 10 compares MATPHOT photometry with residuals (FLUX8: filled diamonds in Fig. 9) with the best corrected circular aperture photometry (FLUX6: filled circles in Fig. 5). The errorbars plotted with the FLUX8 values are the errors estimated by MPDZ for the raw MATPHOT flux estimates (FLUX7: open diamonds in Fig. 9).

We see that although the recorded flux of point sources was corrupted by using lossy detectors with large intrapixel quantum efficiency variations, it is possible to significantly improve the precision of stellar photometry from observations made with such detectors — if the image formation process inside the detector is accurately modeled.

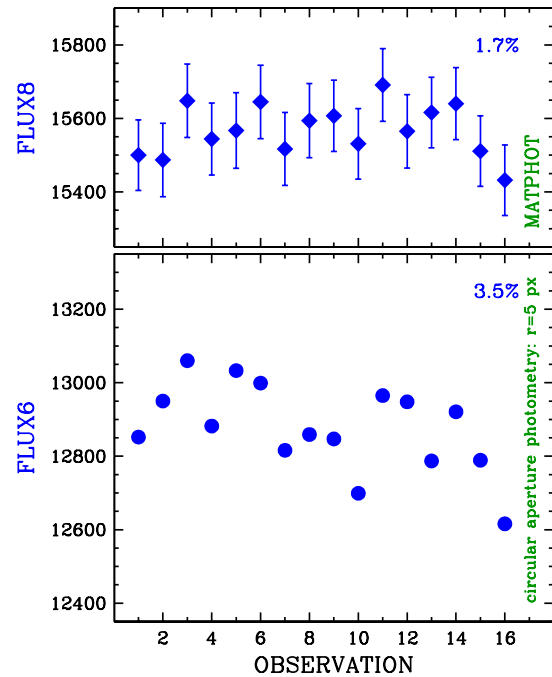


Fig. 10. MATPHOT versus circular aperture photometry.

A very interesting finding of this experiment is that even though the MATPHOT-computed Point Response Functions are not (yet) ideal matches to IRAC Ch1 stellar images, *simple aperture photometry* of stellar observations obtained with IRAC Ch1 *can be significantly improved by simply dividing the measured aperture flux by the MATPHOT-computed volume of the PRF* which is the convolution of the Point Spread Function and the discrete Detector Response Function. Fig. 11 compares the best *uncorrected* circular aperture photometry (FLUX5: open circles in Fig. 5) with those flux values divided by the volume of the best-fit PRF computed by MPDZ. The resultant peak-to-peak spread seen in the top graph of Fig. 11 is **1.9%**



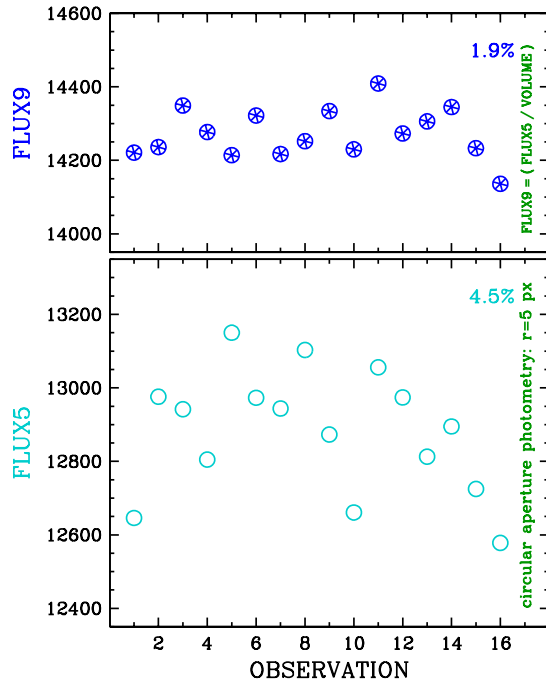


Fig. 11. Raw circular aperture fluxes corrected with MATPHOT-computed PRF volumes.

which is just slightly worse than the **1.7%** spread from the MATPHOT with residual results. This suggests that *aperture* photometry from IRAC Ch1 observations could probably be significantly improved by using a two-dimensional correction function instead of using the radial correction function currently recommended in the IRAC Data Handbook.

The derivation of that two-dimensional correction function would require a detailed analysis of a large number of dithered IRAC Ch1 unsaturated stellar observations. Fortunately, hundreds of suitable observations already exist in the *Spitzer* data archive – many which were obtained during calibration campaigns designed by the IRAC instrument team. Analyzing these observations should enable us to accurately quantify how flux loss may be a function of position within the field of view of IRAC. Comparing this external research effort with the work done by the IRAC Instrument Team should lead to a better understanding of the underlying systematics of IRAC.

## VIII. CONCLUSION

Current near-infrared detector technology can produce space-based astronomical imagers with non-uniform pixel response functions. Large intrapixel quantum efficiency variations can cause significant loss of stellar flux depending on where a star is centered within the central pixel of an undersampled stellar image. This article showed how the precision of stellar photometry from an existing space-based near-infrared camera with a lossy detector can be significantly improved by compensating the apparent loss of stellar flux by accurately modeling the image formation process within the detector.

Much more work remains to be done. However, the possibility of significantly improving the precision and accuracy of space-based near-infrared stellar photometry appears to be excellent. Mitigating the impact of flux loss problems seen in state-of-the-art NASA-grade infrared detectors is still in its early days. Hoffmann's IRAC Ch1 intrapixel QE map [35] was the first attempt by the IRAC Instrument Team to quantify this effect. Derivation of the intrapixel QE map is an iterative process due to the apparent centroid shifting caused by the non-uniform QE variation across a pixel; given an initial estimate of the intrapixel QE map, better positions of the input stellar images can then be determined, which, in turn, enables a better measurement of the intrapixel QE map to be made. A stretch goal of 1% photometric precision might even be achievable with some *existing* space-based cameras using state-of-the-art near-infrared detector technology – if the cameras are sufficiently electronically quiet and stable.

Planning is underway for the post-cryogenic (“warm”) operation of the *Spitzer Space Telescope* which will start around April 2009 after all of the liquid helium has been depleted. Only channels 1 and 2 (3.6 and 4.5 microns) of the Infrared Array Camera will be operational at full sensitivity at that time – providing an unmatched sensitivity from 3 to 5 microns until the James Webb Space telescope is launched. The other channels of all remaining instruments will not operate at the elevated temperatures (25-30K) that the spacecraft will experience during its warm mission phase.

During the past year, I have worked with IRAC Instrument Team to demonstrate that my NASA-funded MATPHOT algorithm for precision stellar photometry and astrometry using discrete Point Spread Functions can yield an improvement in the precision of bright star stellar photometry, obtained from IRAC Ch1 observations, of more than 100% over the best results obtained with aperture photometry using the recommended calibration procedures in the IRAC Data Handbook. This collaborative effort will continue with the goal of developing new calibration procedures for IRAC Ch1 and Ch2 that have the potential of significantly improving the precision of IRAC point-source photometry. This timely research effort is intended to not only enhance the science return of existing IRAC Ch1 and Ch2 observations in the *Spitzer* data archive but also those that will be made during the *Spitzer Warm Mission*.

## ACKNOWLEDGMENT

I wish to thank W. Hoffmann, B. Glaccum, D. Elliott, P. Lowrance, and the rest of the IRAC Instrument Team for their support of this research effort. This work has been supported by grants from the National Aeronautics and Space Administration (NASA), Interagency Order Nos. NNG06EC81I, NNG05EB61I, and S-13811-G, which were awarded by the Applied Information Systems Research (AISR) Program of NASA's Science Mission Directorate.

## REFERENCES

- [1] T. R. Lauer, "The Photometry of Undersampled Point-Spread Functions," *Publications of the Astronomical Society of the Pacific*, vol. 111, pp. 1434–1443, Nov. 1999.
- [2] R. I. Thompson, M. Rieke, G. Schneider, D. C. Hines, and M. R. Corbin, "Initial On-Orbit Performance of NICMOS," *Astrophysical Journal, Letters*, vol. 492, pp. L95–L97, Jan. 1998.
- [3] Schultz, et al., *NICMOS Instrument Handbook, Version 8.0*. Baltimore: STScI, 2005.
- [4] R. N. Hook and A. S. Fruchter, "Dithering, Sampling and Image Reconstruction," *ASP Conf. Ser. 216: Astronomical Data Analysis Software and Systems IX*, pp. 521–530, 2000.
- [5] J. T. Trauger, et al., "The on-orbit performance of WFPC2," *Astrophysical Journal, Letters*, vol. 435, pp. L3–L6, Nov. 1994.
- [6] Heyer, Biretta, et al., *WFPC2 Instrument Handbook, Version 9.0*. Baltimore: STScI, 2004.
- [7] J. A. Holtzman, et al., "The performance and calibration of WFPC2 on the Hubble Space Telescope," *Publications of the Astronomical Society of the Pacific*, vol. 107, pp. 156–178, Feb. 1995.
- [8] J. A. Holtzman, C. J. Burrows, S. Casertano, J. J. Hester, J. T. Trauger, A. M. Watson, and G. Worthey, "The Photometric Performance and Calibration of WFPC2," *Publications of the Astronomical Society of the Pacific*, vol. 107, pp. 1065–1093, Nov. 1995.
- [9] P. B. Stetson, "On the Photometric Consequences of Charge-Transfer Inefficiency in WFPC2," *Publications of the Astronomical Society of the Pacific*, vol. 110, pp. 1448–1463, Dec. 1998.
- [10] A. E. Dolphin, "WFPC2 Stellar Photometry with HSTPHOT," *Publications of the Astronomical Society of the Pacific*, vol. 112, pp. 1383–1396, Oct. 2000.
- [11] B. J. Pritzl, H. A. Smith, P. B. Stetson, M. Catelan, A. V. Sweigart, A. C. Layden, and R. M. Rich, "Hubble Space Telescope Snapshot Study of Variable Stars in Globular Clusters: The Inner Region of NGC 6441," *Astronomical Journal*, vol. 126, pp. 1381–1401, Sep. 2003.
- [12] K. J. Mighell and I. U. Roederer, "Flickering Red Giants in the Ursa Minor Dwarf Spheroidal Galaxy: Detection of Low-Amplitude Variability in Faint Red Giant Branch Stars on 10 Minute Timescales," *Astrophysical Journal, Letters*, vol. 617, pp. L41–L44, Dec. 2004.
- [13] K. J. Mighell, "Stellar photometry and astrometry with discrete point spread functions," *Monthly Notices of the Royal Astronomical Society*, vol. 361, pp. 861–878, Aug. 2005.
- [14] R. A. Muller and A. Buffington, "Real-time correction of atmospherically degraded telescope images through image sharpening," *J. Opt. Soc. Am.*, vol. 64, pp. 1200–1210, 1974.
- [15] I. R. King, "The Profile of a Star Image," *Publications of the Astronomical Society of the Pacific*, vol. 83, pp. 199–201, Apr. 1971.
- [16] J. L. Hora, et al., "Performance of the infrared array camera (IRAC) for SIRTf during instrument integration and test," *Proceedings of the SPIE*, vol. 4850, pp. 83–97, Mar. 2003.
- [17] —, "In-flight performance and calibration of the Infrared Array Camera (IRAC) for the Spitzer Space Telescope," *Proceedings of the SPIE*, vol. 5487, pp. 77–92, Oct. 2004.
- [18] W. F. Hoffmann, J. L. Hora, J. E. Mentzell, C. Marx, and P. Eisenhardt, "Simfit and Focus Diversity: methods for determining the focus of the SIRTf telescope in space without a focus slew," *Proceedings of the SPIE*, vol. 4850, pp. 428–440, 2003.
- [19] G. G. Fazio, et al., "The Infrared Array Camera (IRAC) for the Spitzer Space Telescope," *Astrophysical Journal, Supplement*, vol. 154, pp. 10–17, Sep. 2004.
- [20] I. R. King, "Accuracy of measurement of star images on a pixel array," *Publications of the Astronomical Society of the Pacific*, vol. 95, pp. 163–168, Feb. 1983.
- [21] N. Pogson, "Magnitudes of Thirty-six of the Minor Planets for the first day of each month of the year 1857," *Monthly Notices of the Royal Astronomical Society*, vol. 17, pp. 12–15, Nov. 1856.
- [22] B. W. Kernighan and D. M. Ritchie, *The C Programming Language (2nd Edition)*. New Jersey: Prentice Hall, 1988, (ISBN: 0-131-10362-8).
- [23] R. J. Hanisch, A. Farris, E. W. Greisen, W. D. Pence, B. M. Schlesinger, P. J. Teuben, R. W. Thompson, and A. Warnock, III, "Definition of the Flexible Image Transport System (FITS)," *Astronomy and Astrophysics*, vol. 376, pp. 359–380, Sep. 2001.
- [24] K. J. Mighell, "The MATPHOT Algorithm for Digital Point Spread Function CCD Stellar Photometry," *ASP Conf. Ser. 281: Astronomical Data Analysis Software and Systems XI*, pp. 387–390, 2002.
- [25] M. Abramowitz and I. Stegun, *Handbook of Mathematical Functions with Formulas, Graphs, and Mathematical Tables, Applied Mathematics Series, 55*, eds. M. Abramowitz and I. Stegun. Washington, D.C.: NBS, 1964.
- [26] K. J. Mighell, "MATPHOT algorithm for digital point spread function CCD stellar photometry," *Proceedings of the SPIE*, vol. 4847, pp. 207–216, 2002.
- [27] K. Levenberg, "A Method for the Solution of Certain Problems in Least Squares," *Quarterly of Applied Mathematics*, vol. 2, pp. 164–168, 1944.
- [28] D. Marquardt, "An Algorithm for Least-Squares Estimation of Nonlinear Parameters," *SIAM Journal of Applied Mathematics*, vol. 11, pp. 431–441, 1963.
- [29] K. J. Mighell, "Accurate stellar photometry in crowded fields," *Monthly Notices of the Royal Astronomical Society*, vol. 238, pp. 807–833, May 1989.
- [30] —, "Algorithms for CCD Stellar Photometry," *ASP Conf. Ser. 172: Astronomical Data Analysis Software and Systems VIII*, pp. 317–328, 1999.
- [31] D. Tody, "The IRAF Data Reduction and Analysis System," *Proceedings of the SPIE*, vol. 627, pp. 733–, 1986.
- [32] —, "IRAF in the Nineties," *ASP Conf. Ser. 52: Astronomical Data Analysis Software and Systems II*, pp. 173–183, 1993.
- [33] W. T. Reach, et al., *Infrared Array Camera Data Handbook, Version 3.0 (January 20, 2006)*. Pasadena: SSC, 2006.
- [34] B. Hoffmann, "25 Position Model Pixel Response Functions (PRF) Description and Quality," IRAC/TMo5-014 (Simfit Report 52 Final), 2005.
- [35] —, "Intra-pixel Variation Effect on Aperture Photometry," IRAC/TMo5-028 (Simfit Report 59; Version 2: December 10, 2005), 2005.
- [36] K. J. Mighell, "Innovative image analysis software as a technology driver for advances in space telescope design," *Proceedings of the SPIE*, vol. 6265, p. 6265T, 2006.
- [37] —, "Improving the Precision of Near-Infrared Stellar Photometry by Modeling the Image Formation Process within a Lossy Detector," *Proceedings of the 2006 Advanced Maui Optical and Space Surveillance (AMOS) Technologies Conference*, pp. 201–208, 2006.
- [38] —, "The Lost Flux Method: A New Algorithm for Improving the Precision of Space-Based Near-Infrared Stellar Photometry with Lossy Detectors," *Bulletin of the American Astronomical Society*, vol. 34, p. 1132, 2006.
- [39] —, "The Lost Flux Method: A New Algorithm for Improving the Precision of Space-Based Near-Infrared Stellar Photometry with Lossy Detectors," *ASP Conf. Ser.: Astronomical Data Analysis Software and Systems XVI*, 2007, 4 pages (in press).

## Enhancing the Science Return of the Spitzer Warm Mission<sup>1</sup>

Kenneth Mighell

*National Optical Astronomy Observatory, 950 N. Cherry Ave., Tucson, AZ 85719*

### ABSTRACT

Planning is underway for the post-cryogenic ("warm") operation of the *Spitzer Space Telescope* which will start around April 2009 after all of the liquid helium has been depleted. Only channels 1 and 2 (3.6 and 4.5 microns) of Spitzer's Infrared Array Camera (IRAC) will be operational at full sensitivity at that time -- providing an unmatched sensitivity from 3 to 5 microns until the *James Webb Space Telescope* is launched. The other channels of all remaining instruments will not operate at the elevated temperatures (25-30K) of Spitzer will experience during its warm mission phase. Last year at AMOS 2006, I showed how the recorded flux of bright point sources observed with IRAC Ch1 is corrupted by lossy detectors which have large intrapixel quantum efficiency variations. During the past year, I have worked closely with members of Spitzer's IRAC Instrument Team to demonstrate that my NASA-funded MATPHOT algorithm for precision stellar photometry and astrometry can yield an improvement in the precision of stellar photometry obtained from IRAC Ch1 observations of bright stars of more than 100% over the best results obtained with aperture photometry corrected with the radial correction recommended in the IRAC Data Handbook. I describe some results of an ongoing effort to develop new calibration procedures for IRAC Ch1 and Ch2 which have the potential of significantly improving the precision of IRAC bright point-source photometry. This timely research effort is intended to not only enhance the science return of existing IRAC Ch1 observations in the Spitzer data archive but also those that will be made during the Spitzer Warm Mission.

### 1. SPITZER SPACE TELESCOPE'S WARM MISSION

The *Spitzer Space Telescope* (SST) was launched into an Earth-trailing orbit from the Kennedy Space Flight Center on 2003 August 25 UT (see Fig. 1) [1]. The 85-cm cryogenically cooled beryllium Ritchey-Chretien telescope system operates at temperatures as low as 5.5 K. Planning is underway for the post-cryogenic ("warm") operation of the *Spitzer Space Telescope* which will start around April 2009 after all of the liquid helium has been depleted. Only channels 1 and 2 (3.6 and 4.5 microns) of Spitzer's Infrared Array Camera (IRAC; [2]) will be operational at full sensitivity at that time -- providing an unmatched sensitivity from 3 to 5 microns until the *James Webb Space Telescope* is launched. The other channels of all remaining instruments will not operate at the elevated temperatures (25-30K) of Spitzer will experience during its warm mission phase. This article describe some results of an ongoing effort to develop new calibration procedures for IRAC Ch1 and Ch2 which have the potential of significantly improving the precision of IRAC bright point-source photometry. This timely research effort is intended to not only enhance the science return of existing IRAC Ch1 and Ch2 observations in the Spitzer data archive but also those that will be made during the Spitzer Warm Mission.

---

<sup>1</sup> This work is based on archival data obtained with the *Spitzer Space Telescope*, which is operated by the Jet Propulsion Laboratory, California Institute of Technology under a contract with NASA. Support for this work was provided by an award issued by JPL/Caltech.

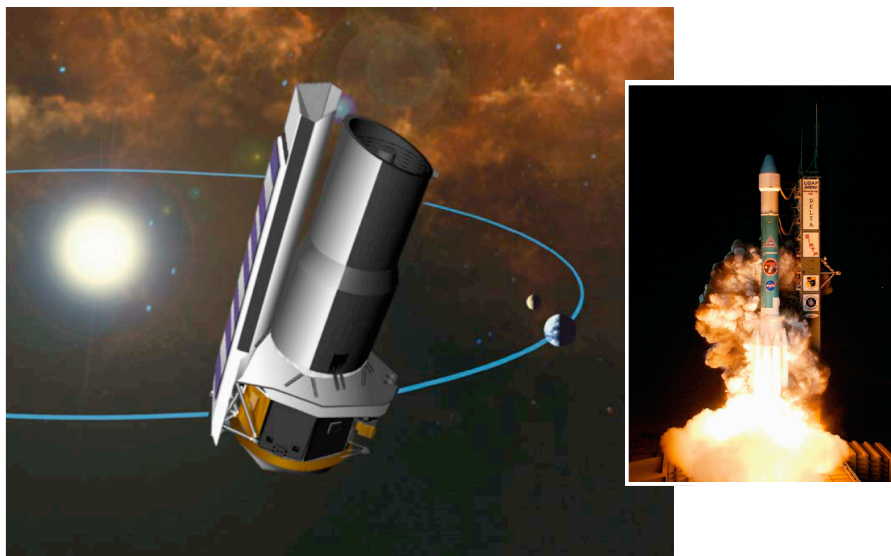


Fig. 1. This artist rendition shows an external view of the *Spitzer Space Telescope* in its Earth-trailing solar orbit. The insert image shows the launch of the SST from the Kennedy Space Flight Center on 2003 August 25 UT [1].

## 2. OBSERVATIONS AND PHOTOMETRIC REDUCTIONS

Sixteen short (0.4 s) calibration observations of the K0 star PPM 9412 were obtained on 2003 October 8 UT with Channel 1 (3.6  $\mu\text{m}$ ) of the Infrared Array Camera onboard the *Spitzer Space Telescope* (see Table 1).

ID	RA_HMS	DEC_DMS	EXPTIME	DATE_OBS	DS_IDENT
1	17h06m11.6s	+73d40m11s	0.4	2003-10-08T11:55:51.356	ads/sa.spitzer#0006875392
2	17h06m11.1s	+73d40m11s	0.4	2003-10-08T12:08:56.748	ads/sa.spitzer#0006876672
3	17h06m10.8s	+73d40m10s	0.4	2003-10-08T12:22:01.538	ads/sa.spitzer#0006876928
4	17h06m10.6s	+73d40m09s	0.4	2003-10-08T12:35:06.524	ads/sa.spitzer#0006877184
5	17h06m11.3s	+73d40m12s	0.4	2003-10-08T12:48:11.510	ads/sa.spitzer#0006877440
6	17h06m10.9s	+73d40m12s	0.4	2003-10-08T13:01:16.496	ads/sa.spitzer#0006877696
7	17h06m10.5s	+73d40m11s	0.4	2003-10-08T13:14:21.489	ads/sa.spitzer#0006877952
8	17h06m10.2s	+73d40m11s	0.4	2003-10-08T13:27:26.471	ads/sa.spitzer#0006878208
9	17h06m11.0s	+73d40m14s	0.4	2003-10-08T13:40:31.472	ads/sa.spitzer#0006878464
10	17h06m10.7s	+73d40m13s	0.4	2003-10-08T13:53:36.446	ads/sa.spitzer#0006878720
11	17h06m10.5s	+73d40m13s	0.4	2003-10-08T14:06:41.436	ads/sa.spitzer#0006878976
12	17h06m10.0s	+73d40m12s	0.4	2003-10-08T14:19:46.422	ads/sa.spitzer#0006879232
13	17h06m11.0s	+73d40m15s	0.4	2003-10-08T14:32:51.423	ads/sa.spitzer#0006879488
14	17h06m10.5s	+73d40m15s	0.4	2003-10-08T15:06:39.788	ads/sa.spitzer#0006879744
15	17h06m10.3s	+73d40m14s	0.4	2003-10-08T15:19:44.785	ads/sa.spitzer#0006880000
16	17h06m10.0s	+73d40m13s	0.4	2003-10-08T15:32:49.763	ads/sa.spitzer#0006880256

Table 1. IRAC Ch1 Observations of PPM 9412.



The IRAC basic calibrated data (BCD) images were retrieved from the Spitzer data archive. These observations were analyzed with the *imexamine* task of NOAO's Image Reduction and Analysis Facility (IRAF; [3–4]) package and a new experimental version of the MATPHOT [5] photometric reduction package, called MPDZ, which uses the following relative intrapixel quantum efficiency (QE) variation map [6] for IRAC Channel 1 (Ch1),

$$\text{intrapix} = \begin{pmatrix} 0.813 & 0.875 & 0.875 & 0.875 & 0.813 \\ 0.875 & 1.000 & 1.000 & 1.000 & 0.875 \\ 0.875 & 1.000 & 1.000 & 1.000 & 0.875 \\ 0.875 & 1.000 & 1.000 & 1.000 & 0.875 \\ 0.813 & 0.875 & 0.875 & 0.875 & 0.813 \end{pmatrix},$$

and a theoretical IRAC Ch1 PSF [7] for the central region of IRAC Ch1 (see Fig. 2).

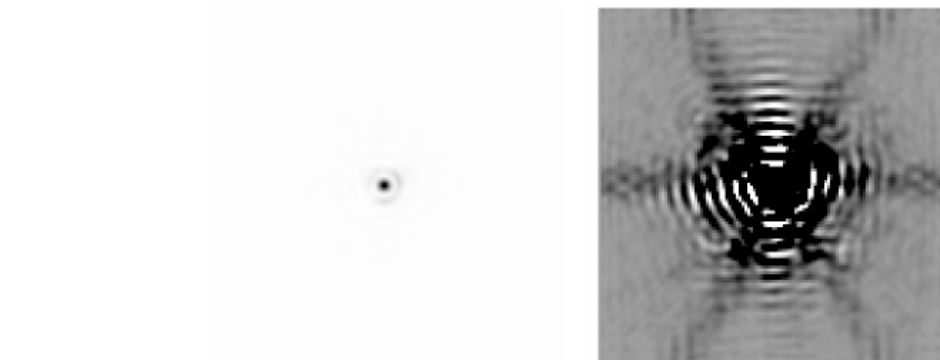


Fig. 2. A theoretical 5x5 supersampled version of the IRAC PSF for the central region of Ch1 [7]. The left side of 4 shows a linear stretch of the PSF and the right side shows a log stretch. Although the PSF appears to be reasonable in the linear stretch, which emphasizes the bright central core, the log stretch shows the numerous weak higher-spatial-frequency features of this very complicated PSF. IRAC Ch1 PSFs are significantly undersampled by the IRAC Ch1 camera [2].

### 3. SQUARE APERTURE PHOTOMETRY

Square aperture photometry with a 21x21 pixel box centered on the star was done using the interactive “m” keyboard command of IRAF's *imexamine* task. Fig. 3 shows a 5.6% peak-to-peak spread in these square aperture flux measurements.

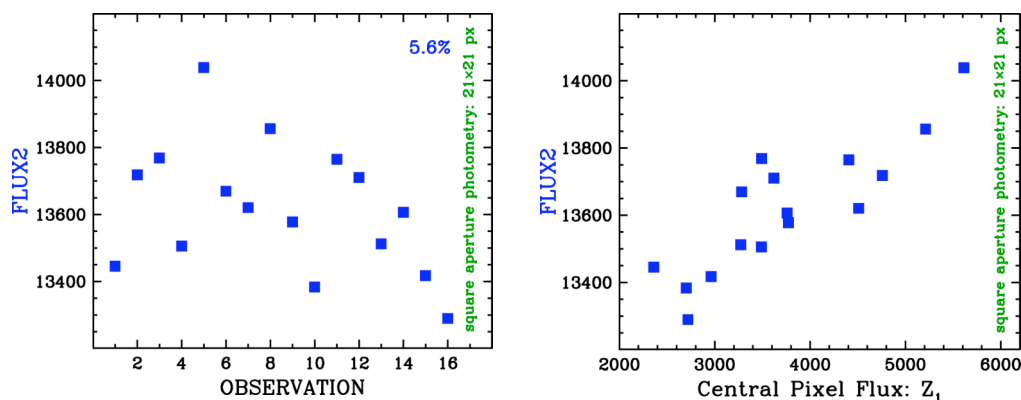


Fig. 3. Square aperture photometry (21x21 pixels)

The variation in flux seen in Fig. 3 is not completely random. The right graph of Fig. 3 shows that the total stellar flux is correlated with the amount of flux found in the central pixel. Examination of the individual observations

reveal that the observations with the most stellar flux have stellar images that are centered in the middle of a pixel while those observations with the least stellar flux are centered on a pixel corner. This same effect is seen in Fig. 4 which is taken from the IRAC Data Handbook [8].

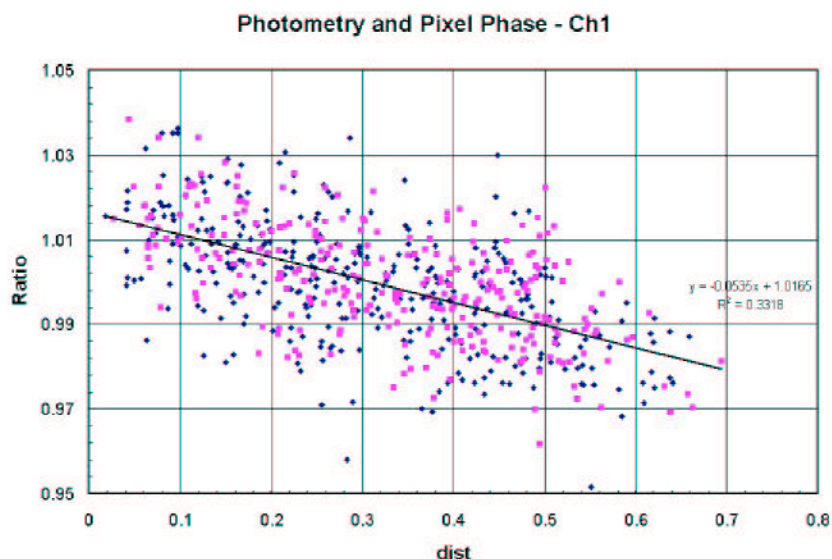


Fig. 4. Normalized measured flux density (y-axis) is plotted against the distance of the source centroid from the center of a pixel (source: Fig. 5.1 of the IRAC Data Handbook [8]).

The flux density of a point source measured from IRAC images depends on the exact location where the peak of the stellar image (the Point Response Function) falls within the central pixel of the stellar image. This effect is due to the variations in the quantum efficiency of a pixel, and combined with the undersampling of the PRF, it is most severe in Channel 1 [8]. The correction can be as much as 4% peak to peak.

#### 4. CIRCULAR APERTURE PHOTOMETRY

Circular aperture photometry centered on the star with a radius of 10 pixels was done using the interactive “a” keyboard command of IRAF’s imexamine task. Fig. 5 shows a 4.5% peak-to-peak spread in the raw circular aperture flux measurements (open circles) with a radius of 5 pixels. Applying the recommended Ch1 flux correction from the IRAC Data Handbook reduces the peak-to-peak spread to 3.5% (filled circles).

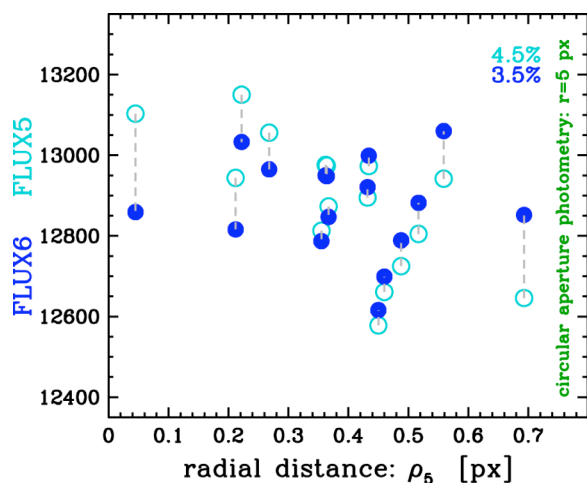


Fig. 5. Circular aperture photometry (radius of 5 pixels)

## 5. MATPHOT SIMULATIONS: PART I

Ten thousand IRAC Ch1 observations of a single star on a flat background were simulated and analyzed with MPDZ. Each stellar observation was simulated using the theoretical 5x5 supersampled IRAC Ch1 PSF shown in Fig. 2; a star with  $10^6$  electrons was located near the center of an field of 60x60 pixels on a flat background of 100 electrons. The horizontal axis of the left graph of Fig. 6 shows the subpixel offset (distance) the center of a star is from the middle of a pixel; stars centered near the middle of a pixel will have small offset values while stars located near the corner of a pixel will have offsets near 0.7 px. The vertical axis of the left graph of Fig. 6 shows the absolute flux ratio of the total fluxes divided by the true flux of  $10^6$  electrons. The cyan points show the *observed* absolute flux ratios and the blue points show the measured absolute flux ratios as reported by MPDZ. Note that while the *average* stellar observation suffered an absolute flux loss of about 9%, stars centered near the middle of a pixel suffered, on average, an absolute flux loss of about 7% as compared to an absolute flux loss of about 11% for stars centered near a pixel corner. It is important to note that *the vertical scatter seen in the observed flux ratios is not random but systematic*; a simple radial correction function can only partially recover the lost flux. The *measured* absolute flux ratios are clustered around unity and are not a function of subpixel offset; the vertical scatter seen in the measured absolute flux ratios is random. By modeling the image formation process within the detector, MPDZ was able to fully recover all of the stellar flux lost due to the non-uniform IRAC Ch1 intrapixel quantum efficiency variations.

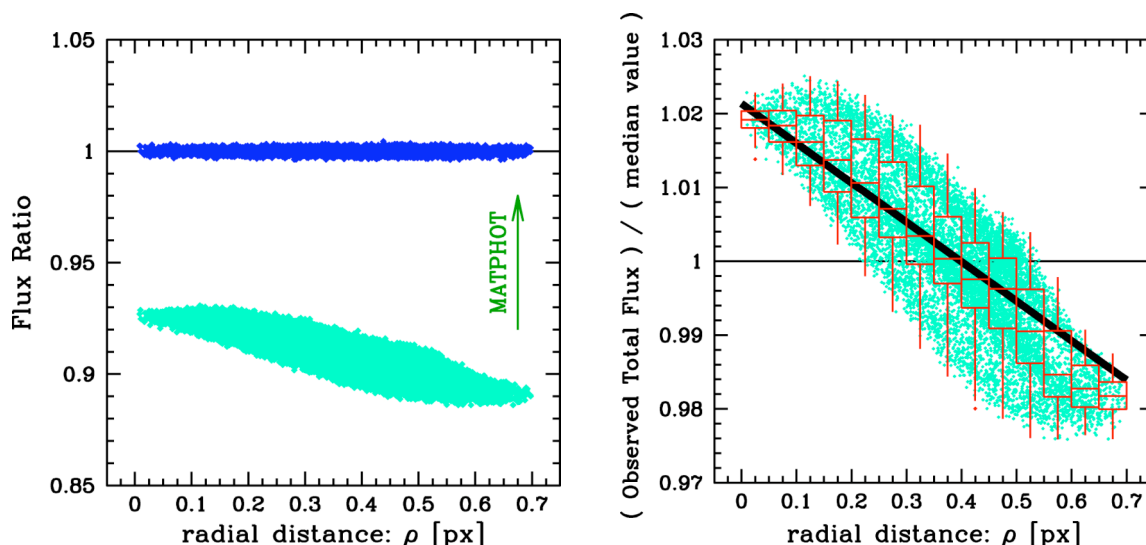


Fig. 6. Results of the MPDZ experiment with simulated IRAC Ch1

The vertical axis of the right graph of Fig. 6 shows the *observed* (apparent) total flux divided by the *median observed* total flux value of all ten thousand stars. The median values of the box-and-whisker plots (the central horizontal bar in each box) range from an excess flux of about 2% for stars centered near the center of a pixel to a flux deficit of about 2% for stars centered near the corner of a pixel. Note that this graph reproduces almost exactly the observed flux loss distribution seen in Fig. 5.1 of the IRAC Data Handbook [8]. One sees that even after the recommended flux correction (thick line of right graph of Fig. 6) is applied an approximate peak-to-peak spread of about 3% would remain for many observations – and that is exactly what is seen in Fig. 5.

## 6. MATPHOT PHOTOMETRY

MATPHOT PSF-fitting photometry was performed on all of the observations using MPDZ with the theoretical 5x5 supersampled IRAC Ch1 PSF shown in Fig. 2. The open diamonds in Fig. 7 show a 5.2% peak-to-peak spread in the raw measured stellar flux values reported by MPDZ.

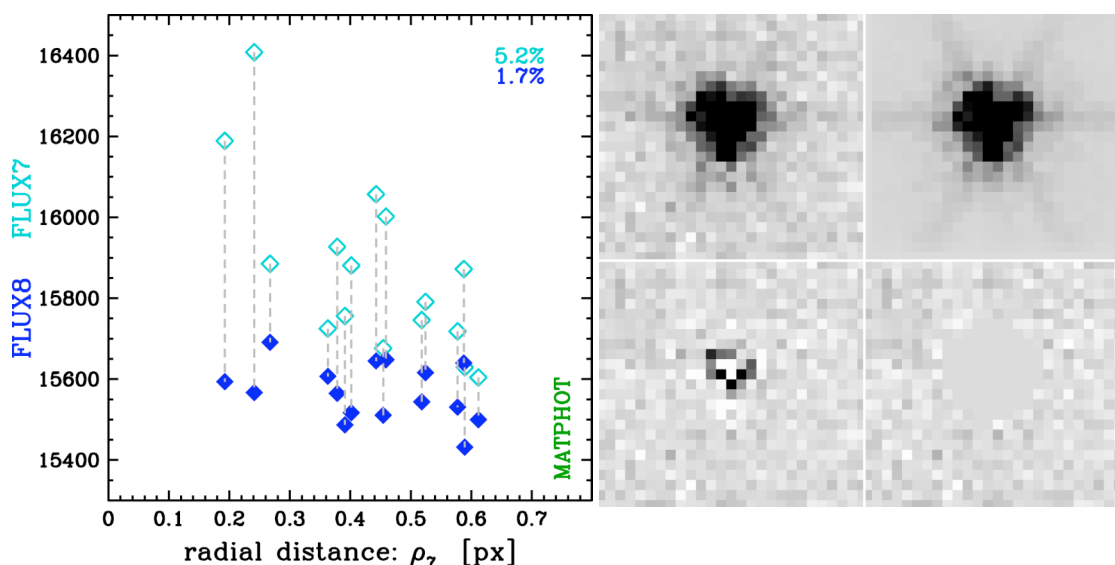


Fig. 7. MATPHOT (MPDZ) photometry

The upper-left image in Fig. 7 shows central portion of the first IRAC Ch1 observation in Table 1. The noiseless best-fit model of the observation is shown in the upper-right image. The residuals remaining after the best-fit model is subtracted from the observation are shown in the lower-left image. The lower-right image is the same as the residual image except that all residuals within a radius of 5 pixels from the fitted center of the star have been set to zero. All of these images are displayed with the same negative linear stretch which was chosen to emphasize the faint features of the stellar image.

The filled diamonds in Fig. 7 show a 1.7% peak-to-peak spread; these flux values are the combination of the raw measured stellar fluxes (open diamonds) with the sum of all of residuals (positive and negative) within a radius of 5 pixels from the fitted center of the star.

MATPHOT with residuals yield an improvement in photometric precision of more than 100% over the best results obtained with aperture photometry. The left graph of Fig. 8 compares MATPHOT photometry with residuals (FLUX8: filled diamonds in Fig. 7) with the best corrected circular photometry (FLUX6: filled circles in Fig. 5). The errorbars plotted with the FLUX8 values are the errors estimated by MPDZ for the raw MATPHOT flux estimates (FLUX7: open diamonds in Fig. 7).

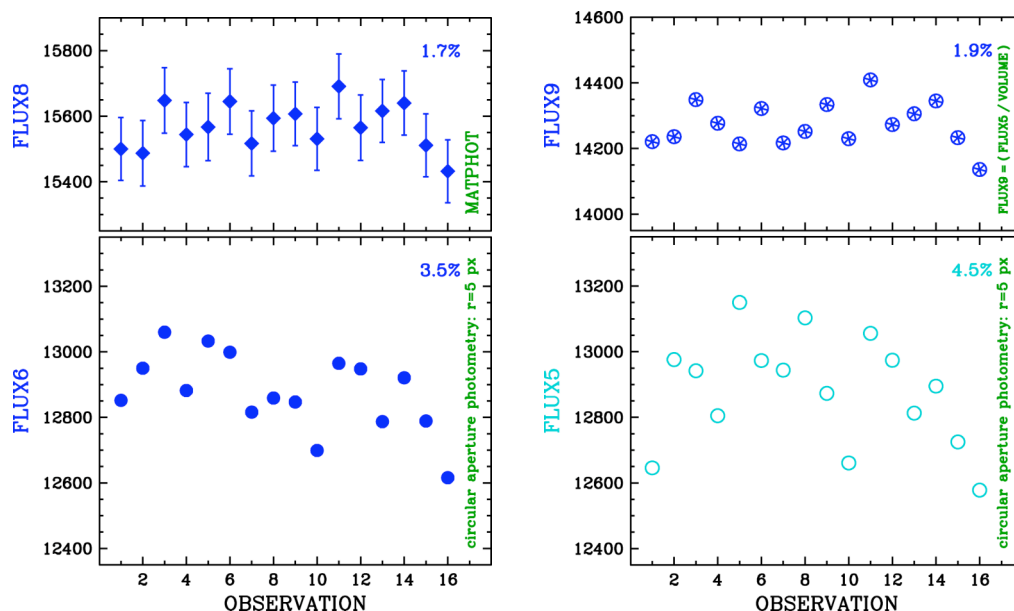


Fig. 8. Comparison between MATPHOT and aperture photometry

We see that although the recorded flux of point sources was corrupted by using lossy detectors with large intrapixel quantum efficiency variations, it is possible to significantly improve the precision of stellar photometry from observations made with such detectors – if the image formation process inside the detector is accurately modeled.

**Simple aperture photometry of stellar observations obtained with IRAC Ch1 can be significantly improved by simply dividing the measured aperture flux with the volume of the Point Response Function (PRF) which is the convolution of the Point Spread Function and the discrete Detector Response Function.** The right graph of Fig. 8 compares the best uncorrected circular photometry (FLUX5: open circles in Fig. 5) with those flux values divided by the volume of the best-fit PRF computed by MPDZ. The resultant peak-to-peak spread is 1.9% which is just slightly worse than the 1.7% spread from the MATPHOT with residual results. This suggests that aperture photometry from IRAC Ch1 observations could probably be significantly improved by using a two-dimensional correction function instead of using the radial correction function currently recommended in the IRAC Data Handbook. The derivation of that two-dimensional correction function would require a detailed analysis of a large number of dithered IRAC Ch1 unsaturated stellar observations.

## 7. MATPHOT SIMULATIONS: PART II

I determined a new two-dimensional flux correction based on the computed MATPHOT Point Response Function (PRF) volumes of 100,000 artificial stellar observations. Median values were determined on a 11x11 grid of the central pixel of the PRF. Columns 1 and 2 of Table 2 give, respectively, the pixel offset from the center of the pixel in the  $x$  and  $y$  directions in pixel units; the third column gives the radial distance from the center of the pixel in pixel units. Columns 5 and 6 give the respective subpixel offset in the  $x$  and  $y$  directions; the values range from -5 to 5 with the central subpixel having  $idx$  and  $idy$  values of zero. Column 6 gives the new flux correction which can be compared with the value given in last column ( $idhcorr$ ) which is the recommended flux correction given in the IRAC Data Handbook.



Table 2. New IRAC Ch1 Aperture Correction (column 6).

#	dx	dy	dr	idx	idy	newcorr	idhcorr
-0.4545	-0.4545	0.6428	-5	-5	0.9822	0.9870	
-0.3636	-0.4545	0.5821	-4	-5	0.9823	0.9902	
-0.2727	-0.4545	0.5301	-3	-5	0.9856	0.9930	
-0.1818	-0.4545	0.4896	-2	-5	0.9909	0.9952	
-0.0909	-0.4545	0.4635	-1	-5	0.9962	0.9965	
0.0000	-0.4545	0.4545	0	-5	1.0005	0.9970	
0.0909	-0.4545	0.4635	1	-5	1.0019	0.9965	
0.1818	-0.4545	0.4896	2	-5	1.0005	0.9952	
0.2727	-0.4545	0.5301	3	-5	0.9962	0.9930	
0.3636	-0.4545	0.5821	4	-5	0.9905	0.9902	
0.4545	-0.4545	0.6428	5	-5	0.9851	0.9870	
-0.4545	-0.3636	0.5821	-5	-4	0.9877	0.9902	
-0.3636	-0.3636	0.5143	-4	-4	0.9877	0.9938	
-0.2727	-0.3636	0.4545	-3	-4	0.9912	0.9970	
-0.1818	-0.3636	0.4066	-2	-4	0.9962	0.9996	
-0.0909	-0.3636	0.3748	-1	-4	1.0019	1.0013	
0.0000	-0.3636	0.3636	0	-4	1.0060	1.0019	
0.0909	-0.3636	0.3748	1	-4	1.0074	1.0013	
0.1818	-0.3636	0.4066	2	-4	1.0060	0.9996	
0.2727	-0.3636	0.4545	3	-4	1.0017	0.9970	
0.3636	-0.3636	0.5143	4	-4	0.9957	0.9938	
0.4545	-0.3636	0.5821	5	-4	0.9903	0.9902	
-0.4545	-0.2727	0.5301	-5	-3	0.9937	0.9930	
-0.3636	-0.2727	0.4545	-4	-3	0.9939	0.9970	
-0.2727	-0.2727	0.3857	-3	-3	0.9972	1.0007	
-0.1818	-0.2727	0.3278	-2	-3	1.0024	1.0038	
-0.0909	-0.2727	0.2875	-1	-3	1.0082	1.0060	
0.0000	-0.2727	0.2727	0	-3	1.0122	1.0068	
0.0909	-0.2727	0.2875	1	-3	1.0140	1.0060	
0.1818	-0.2727	0.3278	2	-3	1.0123	1.0038	
0.2727	-0.2727	0.3857	3	-3	1.0078	1.0007	
0.3636	-0.2727	0.4545	4	-3	1.0018	0.9970	
0.4545	-0.2727	0.5301	5	-3	0.9964	0.9930	
-0.4545	-0.1818	0.4896	-5	-2	0.9988	0.9952	
-0.3636	-0.1818	0.4066	-4	-2	0.9990	0.9996	
-0.2727	-0.1818	0.3278	-3	-2	1.0023	1.0038	
-0.1818	-0.1818	0.2571	-2	-2	1.0077	1.0076	
-0.0909	-0.1818	0.2033	-1	-2	1.0133	1.0105	
0.0000	-0.1818	0.1818	0	-2	1.0176	1.0116	
0.0909	-0.1818	0.2033	1	-2	1.0192	1.0105	
0.1818	-0.1818	0.2571	2	-2	1.0175	1.0076	
0.2727	-0.1818	0.3278	3	-2	1.0130	1.0038	
0.3636	-0.1818	0.4066	4	-2	1.0074	0.9996	
0.4545	-0.1818	0.4896	5	-2	1.0017	0.9952	
-0.4545	-0.0909	0.4635	-5	-1	1.0011	0.9965	
-0.3636	-0.0909	0.3748	-4	-1	1.0014	1.0013	
-0.2727	-0.0909	0.2875	-3	-1	1.0047	1.0060	
-0.1818	-0.0909	0.2033	-2	-1	1.0101	1.0105	
-0.0909	-0.0909	0.1286	-1	-1	1.0158	1.0145	
0.0000	-0.0909	0.0909	0	-1	1.0200	1.0165	
0.0909	-0.0909	0.1286	1	-1	1.0216	1.0145	
0.1818	-0.0909	0.2033	2	-1	1.0201	1.0105	
0.2727	-0.0909	0.2875	3	-1	1.0154	1.0060	
0.3636	-0.0909	0.3748	4	-1	1.0095	1.0013	
0.4545	-0.0909	0.4635	5	-1	1.0039	0.9965	
-0.4545	0.0000	0.4545	-5	0	1.0004	0.9970	
-0.3636	0.0000	0.3636	-4	0	1.0006	1.0019	

-0.2727	0.0000	0.2727	-3	0	1.0036	1.0068
-0.1818	0.0000	0.1818	-2	0	1.0088	1.0116
-0.0909	0.0000	0.0909	-1	0	1.0147	1.0165
0.0000	0.0000	0.0000	0	0	1.0188	1.0213
0.0909	0.0000	0.0909	1	0	1.0206	1.0165
0.1818	0.0000	0.1818	2	0	1.0188	1.0116
0.2727	0.0000	0.2727	3	0	1.0145	1.0068
0.3636	0.0000	0.3636	4	0	1.0086	1.0019
0.4545	0.0000	0.4545	5	0	1.0031	0.9970
-0.4545	0.0909	0.4635	-5	1	0.9963	0.9965
-0.3636	0.0909	0.3748	-4	1	0.9963	1.0013
-0.2727	0.0909	0.2875	-3	1	0.9994	1.0060
-0.1818	0.0909	0.2033	-2	1	1.0047	1.0105
-0.0909	0.0909	0.1286	-1	1	1.0103	1.0145
0.0000	0.0909	0.0909	0	1	1.0146	1.0165
0.0909	0.0909	0.1286	1	1	1.0161	1.0145
0.1818	0.0909	0.2033	2	1	1.0145	1.0105
0.2727	0.0909	0.2875	3	1	1.0101	1.0060
0.3636	0.0909	0.3748	4	1	1.0044	1.0013
0.4545	0.0909	0.4635	5	1	0.9988	0.9965
-0.4545	0.1818	0.4896	-5	2	0.9901	0.9952
-0.3636	0.1818	0.4066	-4	2	0.9902	0.9996
-0.2727	0.1818	0.3278	-3	2	0.9933	1.0038
-0.1818	0.1818	0.2571	-2	2	0.9983	1.0076
-0.0909	0.1818	0.2033	-1	2	1.0040	1.0105
0.0000	0.1818	0.1818	0	2	1.0078	1.0116
0.0909	0.1818	0.2033	1	2	1.0099	1.0105
0.1818	0.1818	0.2571	2	2	1.0082	1.0076
0.2727	0.1818	0.3278	3	2	1.0037	1.0038
0.3636	0.1818	0.4066	4	2	0.9981	0.9996
0.4545	0.1818	0.4896	5	2	0.9928	0.9952
-0.4545	0.2727	0.5301	-5	3	0.9838	0.9930
-0.3636	0.2727	0.4545	-4	3	0.9839	0.9970
-0.2727	0.2727	0.3857	-3	3	0.9873	1.0007
-0.1818	0.2727	0.3278	-2	3	0.9922	1.0038
-0.0909	0.2727	0.2875	-1	3	0.9976	1.0060
0.0000	0.2727	0.2727	0	3	1.0016	1.0068
0.0909	0.2727	0.2875	1	3	1.0036	1.0060
0.1818	0.2727	0.3278	2	3	1.0019	1.0038
0.2727	0.2727	0.3857	3	3	0.9977	1.0007
0.3636	0.2727	0.4545	4	3	0.9920	0.9970
0.4545	0.2727	0.5301	5	3	0.9866	0.9930
-0.4545	0.3636	0.5821	-5	4	0.9798	0.9902
-0.3636	0.3636	0.5143	-4	4	0.9798	0.9938
-0.2727	0.3636	0.4545	-3	4	0.9830	0.9970
-0.1818	0.3636	0.4066	-2	4	0.9881	0.9996
-0.0909	0.3636	0.3748	-1	4	0.9936	1.0013
0.0000	0.3636	0.3636	0	4	0.9978	1.0019
0.0909	0.3636	0.3748	1	4	0.9991	1.0013
0.1818	0.3636	0.4066	2	4	0.9978	0.9996
0.2727	0.3636	0.4545	3	4	0.9937	0.9970
0.3636	0.3636	0.5143	4	4	0.9879	0.9938
0.4545	0.3636	0.5821	5	4	0.9824	0.9902
-0.4545	0.4545	0.6428	-5	5	0.9787	0.9870
-0.3636	0.4545	0.5821	-4	5	0.9787	0.9902
-0.2727	0.4545	0.5301	-3	5	0.9818	0.9930
-0.1818	0.4545	0.4896	-2	5	0.9873	0.9952
-0.0909	0.4545	0.4635	-1	5	0.9927	0.9965
0.0000	0.4545	0.4545	0	5	0.9969	0.9970
0.0909	0.4545	0.4635	1	5	0.9982	0.9965

0.1818	0.4545	0.4896	2	5	0.9969	0.9952
0.2727	0.4545	0.5301	3	5	0.9925	0.9930
0.3636	0.4545	0.5821	4	5	0.9868	0.9902
0.4545	0.4545	0.6428	5	5	0.9814	0.9870

Fig. 9 shows the new two-dimensional correction (121 blue points) with respect to the standard radial correction (black line) for the new 100,000 simulated observations. Note how much better the new flux correction samples the “cloud” of relative flux loss measurements than the standard flux correction recommended by the IRAC Data Handbook.

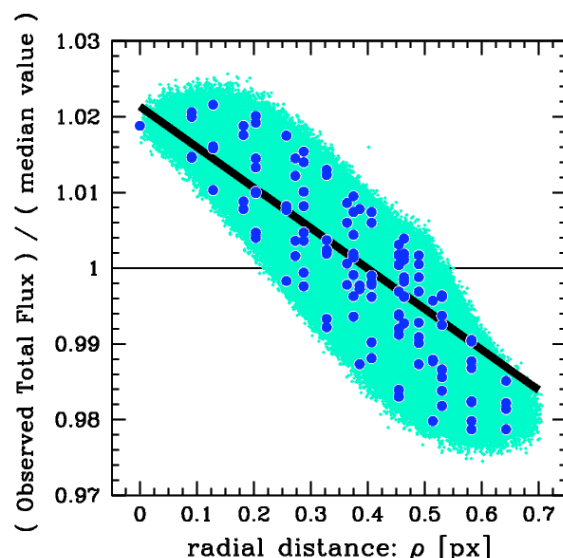


Fig. 9. Comparison of the new flux correction (121 blue points) with the radial correction (black line) in the IRAC Data Handbook.

## 8. APPLICATION OF THE NEW FLUX CORRECTION

Fig. 10 is a new version of Fig. 5 with the red points showing the application of the new flux correction based on centroid positions determined from aperture photometry. I expected to see a peak-to-peak variation of about 2% but the measured variation was 3%. So what went wrong?

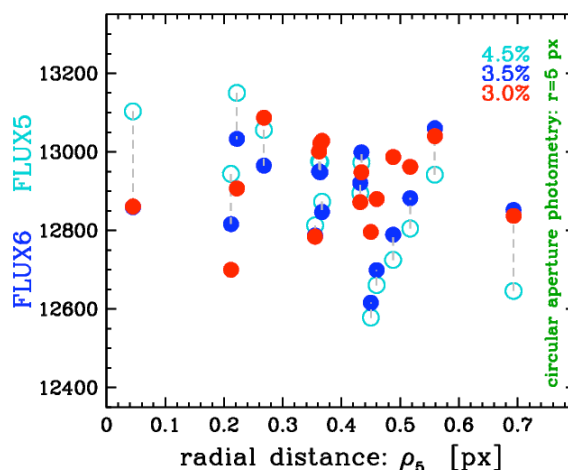


Fig. 10. Circular aperture photometry (radius of 5 pixels) with the new flux correction (red filled circles) based on positions from aperture photometry

Fig. 11 shows that systematic correction errors of 1% are not uncommon because the *wrong position* (from aperture photometry) *was used*! The *measured position*, based on the intensity-weighted mean centroid, can be *systematically off* by as much as *one-sixth of a pixel* (0.2 arcsec) from the *true position* due to nonuniform intrapixel quantum efficiency variation. Note that the peak of the new flux correction is *not* in the center of the central pixel; this is probably due to the convolution of the asymmetric IRAC PSF (due mainly to trefoil aberration) with the nonuniform intrapixel quantum efficiency map.

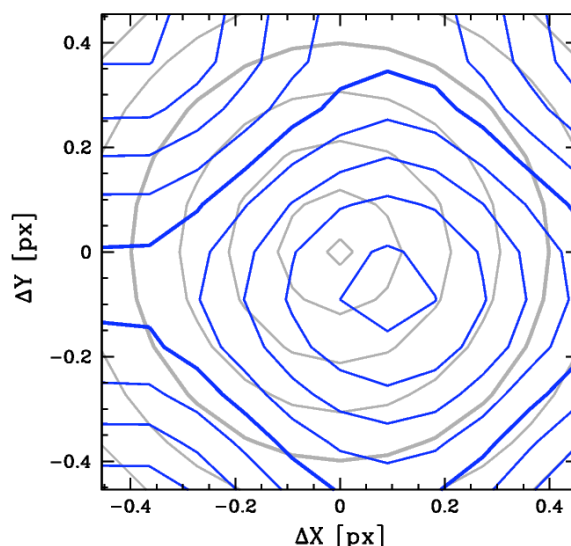


Fig. 11. Comparison of the new flux correction (blue contours) with the flux correction from the IRAC Data Handbook (gray contours). The contours of the standard correction range from 0.99 to 1.02 in steps of 0.005 (0.5%); the contours of the new correction range from 0.98 to 1.02 in steps of 0.005.

Better positions should give better corrections. So... make better centroid measurements using knowledge about the nonuniform intrapixel quantum efficiency variation – say, for example, as determined using MATPHOT. Fig. 12 is a new version of Fig. 10 with the orange diamonds showing the application of the new flux correction based on centroid positions determined from MAPHOT photometry. *The measured peak-to-peak variation is 1.7% which matches the variations found using MATPHOT photometry with residuals.*

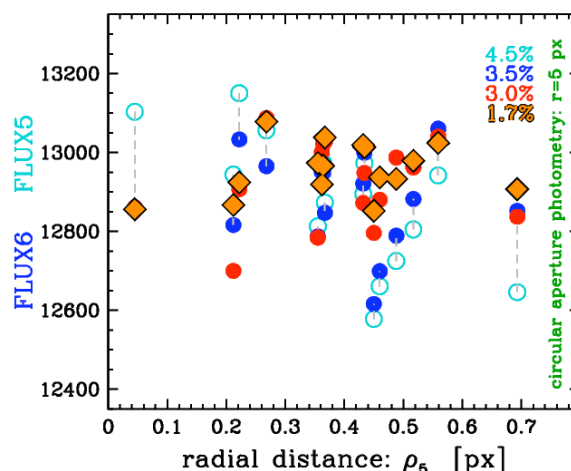


Fig. 12. Circular aperture photometry (radius of 5 pixels) with the new flux correction (red filled circles) based on positions from MATPHOT photometry.

**The new two-dimensional flux correction yields an improvement of 100% over the standard correction given in the IRAC Data Handbook when given accurate centroid estimates.**

## 9. SUMMARY AND DISCUSSION

This detailed analysis of multiple observations of a single bright isolated star obtained with Channel 1 of the *Spitzer Space Telescope*'s Infrared Array Camera (IRAC) instrument yields an improvement in photometric precision of more than 100% over the best results obtained with aperture photometry. The improvement is achieved by accurately modeling the image formation process within lossy detectors that exhibit large intrapixel quantum efficiency variations.

Mitigating the impact of flux loss problems seen in state-of-the-art NASA-grade infrared detectors is still in its early days. Hoffmann's IRAC Ch1 intrapixel QE map is the *first attempt* by the IRAC team to quantify this effect. Derivation of the intrapixel QE map is an *iterative process* due to the apparent centroid shifting caused by the non-uniform QE variation across a pixel; given an initial estimate of the intrapixel QE map, better positions of the input stellar images can then be determined, which, in turn, enables a better measurement of the intrapixel QE map to be made

Much more work remains to be done. However, the possibility of significantly improving the precision and accuracy of space-based near-infrared stellar photometry and astrometry appears to be excellent.

Work has recently begun with the IRAC Instrument Team on a *SST Cycle 4* archival grant (*Improving the Photometric Precision of IRAC Channels 1 and 2*) which will investigate the development of new calibration procedures for IRAC Ch1 and Ch2 that have the potential of significantly improving the precision of IRAC point-source photometry. This timely research effort is intended to not only enhance the science return of existing IRAC Ch1 and Ch2 observations in the *Spitzer Data Archive* but also those that will be made in the future during the *Spitzer Warm Mission*.

I wish to thank Bill Glaccum, Bill Hoffmann, David Elliott, Patrick Lowrance, and the rest of the IRAC team for their support of this research effort. This work has been supported by a grant from the National Aeronautics and Space Administration (NASA), Interagency Order No. NNG06EC81I, which was awarded by the Applied Information Systems Research (AISR) Program of NASA's Science Mission Directorate.

## 10. REFERENCES

1. Gehrz, R. D., The NASA Spitzer Space Telescope, Review of Scientific Instruments, Vol. 78, 011302:1-38, 2007.
2. Fazio, G. G., et al., The Infrared Array Camera (IRAC) for the Spitzer Space Telescope, ApJS, Vol. 154, 10-17, 2004.
3. Tody, D., The *IRAF* Data Reduction and Analysis System, *Instrumentation in Astronomy VI*, Proceedings of the SPIE, Vol. 627, 733, 1986.
4. Tody, D., IRAF in the Nineties, *Astronomical Data Analysis Software and Systems II*, ASP Conf. Ser. 52, 173, 1993.
5. Mighell, K. J., Stellar photometry and astrometry with discrete point spread functions, MNRAS, Vol. 361, 861-878, 2005.
6. Hoffmann, B., Intra-pixel Variation Effect on Aperture Photometry, IRAC/TMo5-028 (Simfit Report 59; Version 2; December 10, 2005), 2005.
7. Hoffmann, B., 25 Position Model Pixel Repsonse Functions (PRF) Description and Quality, IRAC/TMo5-014 Simfit Report 52; September 3, 2005), 2005.
8. Reach, W. T., et al., Infrared Array Camera Data Handbook (Version 3.0; January 20, 2006), 2006.



## **The Lost Flux Method: A New Algorithm for Improving the Precision of Space-Based Near-Infrared Stellar Photometry with Lossy Detectors**

Kenneth J. Mighell

*National Optical Astronomy Observatory, Tucson, AZ, USA*

**Abstract.** Current infrared detector technology can produce imagers with non-uniform intra-pixel response functions. Cameras based on such detectors can have large systematic errors in the measurement of the total stellar flux. Although this problem can be mitigated by oversampling the stellar image, many near-infrared cameras are undersampled in order to achieve a large field of view. The combination of undersampling stellar images with non-uniform detectors is currently diminishing some of the potential science return of some infrared imagers onboard the *Hubble Space Telescope* and the *Spitzer Space Telescope*. Although the recorded flux and position of point sources is corrupted by using detectors with non-uniform intrapixel response functions, it is still possible to achieve excellent stellar photometry and astrometry—if the image formation process inside the detector is accurately modeled. A new analysis algorithm called the *Lost Flux Method* is described and used to demonstrate how the precision of stellar photometry from an existing space-based near-infrared camera with a lossy detector can be significantly improved. Multiple observations of a single bright isolated star obtained with Channel 1 of the *Spitzer Space Telescope* Infrared Array Camera (IRAC) instrument are analyzed with the Lost Flux Method which yields an improvement in photometric precision of more than 100% over the best results obtained with aperture photometry.

### **1. Photometry and Astrometry with Discrete PSFs**

The MATPHOT algorithm for precise and accurate stellar photometry and astrometry with discrete (sampled) point-spread functions (PSFs) was described in detail by Mighell (2005). The current C-language implementation of the MATPHOT algorithm works with user-provided discrete PSFs consisting of a numerical table represented by a matrix in the form of a FITS image (Hanisch et al. 2001). Discrete PSFs are shifted within an observational model using a 21-pixel-wide damped sinc function and position partial derivatives are computed using a five-point numerical differentiation formula. Precise and accurate stellar photometry and astrometry are achieved with undersampled charge coupled device (CCD) observations by using supersampled discrete PSFs that are sampled 2, 3, or more times more finely than the observational data. Although these numerical techniques are not mathematically perfect, they are sufficiently accurate for precision stellar photometry and astrometry due to photon noise which is present in all astronomical imaging observations. The current photometric re-

duction code<sup>1</sup> is based on a robust implementation of the Levenberg-Marquardt method of nonlinear least-squares minimization (Levenberg 1944; Marquardt 1963; Mighell 1989, 1999). Detailed analysis of simulated *James Webb Space Telescope* observations demonstrate that millipixel relative astrometry and millimagnitude photometric precision should be achievable with complicated space-based discrete PSFs (Mighell 2005).

## 2. Observations and Photometric Reductions

Sixteen short (0.4 s) calibration observations of the K0-class star PPM 9412 (a.k.a. HIP 6378) were obtained<sup>2</sup> on 2003 October 8 UT with Channel 1 (3.6  $\mu\text{m}$ ) of the Infrared Array Camera (IRAC; Fazio et al. 2004) on-board the *Spitzer Space Telescope*. The IRAC basic calibrated data (BCD) images were retrieved from the *Spitzer* data archive with the kind assistance of IRAC team member B. Glaccum. These observations were analyzed with the *imexamine* task of NOAO's Image Reduction and Analysis Facility (IRAF; Tody 1993 and references therein) package and a new experimental version of MATPHOT, called MPDZ, which uses the following relative intrapixel quantum efficiency (QE) variation map for IRAC Channel 1 (Ch1),

$$\text{intrapix} = \begin{pmatrix} 0.813 & 0.875 & 0.875 & 0.875 & 0.813 \\ 0.875 & 1.000 & 1.000 & 1.000 & 0.875 \\ 0.875 & 1.000 & 1.000 & 1.000 & 0.875 \\ 0.875 & 1.000 & 1.000 & 1.000 & 0.875 \\ 0.813 & 0.875 & 0.875 & 0.875 & 0.813 \end{pmatrix}$$

(Hoffmann 2005a), and a theoretical IRAC Ch1 PSF for the central region of IRAC Ch1 (Hoffmann 2005b). MATPHOT models the image formation process within the detector by convolving the PSF with the discrete Detector Response Function (DRF) which, in this case, is based on the relative intrapixel QE map given above.

## 3. Square Aperture Photometry

Square aperture photometry with a  $21 \times 21$  pixel box centered on the star was done using the interactive “m” keyboard command of IRAF's *imexamine* task. A 5.6% peak-to-peak spread was seen in these square aperture flux measurements. A non-random variation in flux is quite apparent in these 16 IRAC Ch1 observations: the total stellar flux measured is strongly correlated with the amount of flux found in the central pixel. Examination of the individual observations revealed that the observations with the most stellar flux have stellar images that are centered in the middle of a pixel while those observations with the least stellar flux are centered on a pixel corner. This effect, shown graphically in Fig. 5.1 of the IRAC Data Handbook, is due to the combination of large quantum

<sup>1</sup>All source code and documentation for MATPHOT is available at this website: <http://www.noao.edu/staff/mighell/matphot>

<sup>2</sup>Observations: ads/sa.spitzer#00068nnnnn where nnnnn is 75392, 76672, 76928, 77184, 77440, 77696, 77952, 78208, 78464, 78720, 78976, 79232, 79488, 79744, 80000, 80256.

efficiency variations within individual pixels and the undersampling of the PSF by the DRF, is most severe in Channel 1 ( $3.6\ \mu\text{m}$ ) where the correction can be as much as 4% peak to peak (Reach et al. 2006).

#### 4. Circular Aperture Photometry

Circular aperture photometry centered on the star with a radius of 10 pixels was done using the interactive “a” keyboard command of IRAFs *imexamine* task. A 5.3% peak-to-peak spread was seen in the raw circular aperture flux measurements. Applying the recommended Ch1 flux correction from the IRAC Data Handbook (Reach et al. 2006) only slightly reduces the peak-to-peak spread to 4.9%. Reducing the aperture radius to just 5 pixels does improve the photometric precision; a 4.5% peak-to-peak spread was seen in the raw circular aperture flux measurements which reduces to 3.5% when the recommended Ch1 flux correction was applied. This is the best that aperture photometry can do with these observations.

#### 5. MATPHOT Photometry

MATPHOT PSF-fitting photometry was performed on all of the observations using MPDZ with a theoretical  $5 \times 5$  supersampled IRAC Ch1 PSF kindly provided by IRAC team member B. Hoffmann (see Hoffmann 2005b). The raw measured stellar flux values reported by MPDZ had a 5.2% peak-to-peak spread. However, when those flux values are combined with the sum of all of the residuals (positive and negative differences between the data and the best-fit model) within a radius of 5 pixels from the fitted center of the star, then the photometry has a 1.7% peak-to-peak spread—an improvement in photometric precision of more than 100% over the best results obtained with aperture photometry (see left graph of Figure 1). This experiment has demonstrated that even if the recorded flux of point sources is corrupted by using lossy detectors with large intrapixel quantum efficiency variations, it is practical to significantly improve the precision of stellar photometry from observations made with such detectors by accurately modeling the image formation process within the detector.

A very interesting finding of this experiment is that simple aperture photometry of stellar observations obtained with IRAC Ch1 can be significantly improved by simply dividing the measured aperture flux with the MPDZ-computed volume of the Point Response Function (PRF) which is the convolution of the PSF with the discrete DRF. When the best *uncorrected* circular aperture flux values were divided by the volume of the best-fit PRF computed by MPDZ, the photometric precision improved from the 4.5% peak-to-peak value (reported above) to just 1.9% (see right graph of Figure 1) which is just slightly worse than the 1.7% spread result from MPDZ with residuals. This suggests that aperture photometry from IRAC Ch1 observations could probably be significantly improved by using a two-dimensional correction function instead of using the radial correction function currently recommended in the IRAC Data Handbook. The derivation of that two-dimensional correction function would require a detailed analysis of a large number of dithered IRAC Ch1 unsaturated stellar observations.

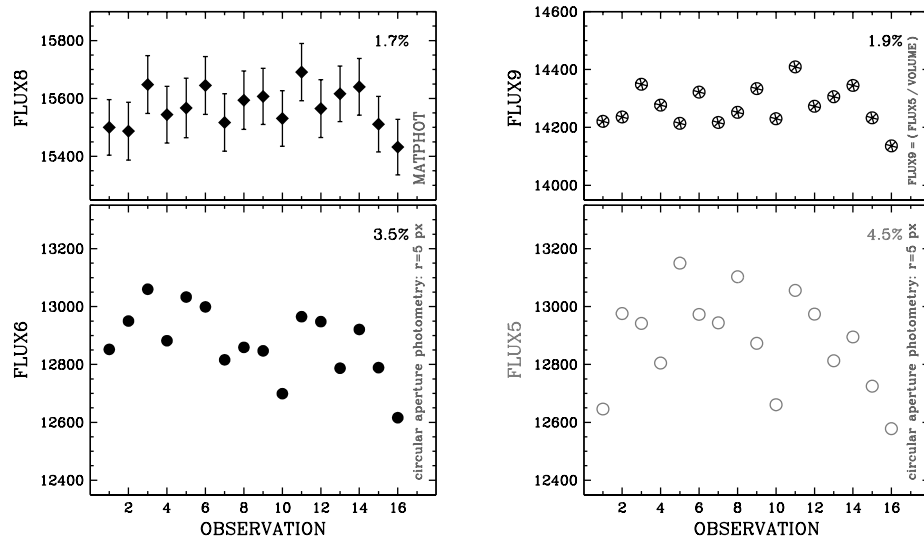


Figure 1. MATPHOT (MPDZ) photometry with residuals versus circular aperture photometry with a radius of 5 pixels.

**Acknowledgments.** I wish to thank B. Glaccum, W. Hoffmann, D. Elliott, P. Lowrance, and the rest of the IRAC team for their support of this research effort. This work has been supported by a grant from the National Aeronautics and Space Administration (NASA), Interagency Order No. NNG06EC81I, which was awarded by the NASA Applied Information Systems Research Program.

## References

- Fazio, G. G., et al. 2004, *ApJS*, 154, 10  
 Hanisch, R. J., et al. 2001, *A&A*, 376, 359  
 Hoffmann, B. 2005a, IRAC/TMo5-028 (Pasadena, CA: Spitzer Science Center)  
 Hoffmann, B. 2005b, IRAC/TMo5-014, (Pasadena, CA: Spitzer Science Center)  
 Levenberg, K. 1944, *Quarterly of Applied Mathematics*, 2, 164  
 Marquardt, D. 1963, *SIAM Journal of Applied Mathematics*, 11, 431  
 Mighell, K. J. 1989, *MNRAS*, 238, 807  
 Mighell, K. J. 1999, in *ASP Conf. Ser. 172, ADASS VIII*, ed. D. M. Mehringer, R. L. Plante, & D. A. Roberts (San Francisco: ASP), 317  
 Mighell, K. J. 2005, *MNRAS*, 361, 861  
 Reach, W. T., et al. 2006, *Infrared Array Camera Data Handbook (Version 3.0: Pasadena, CA: Spitzer Science Center)*  
 Tody, D. 1993, in *ASP Conf. Ser. 52, ADASS II*, ed. R. J. Hanisch, R. J. V. Brissenden, & J. Barnes (San Francisco: ASP), 173